A localized momentum constraint for non-equilibrium molecular dynamics simulations

E. R. Smith, D. M. Heyes, D. Dini, and T. A. Zaki

Articles you may be interested in

Efficient hybrid non-equilibrium molecular dynamics - Monte Carlo simulations with symmetric momentum reversal
J. Chem. Phys. **141**, 114107 (2014); 10.1063/1.4895516

Brownian dynamics simulations of nanosheet solutions under shear
J. Chem. Phys. **141**, 024905 (2014); 10.1063/1.4884821

Rigid body dynamics approach to Stokesian dynamics simulations of nonspherical particles
J. Chem. Phys. **132**, 174107 (2010); 10.1063/1.3358330

Large-scale molecular dynamics simulations of normal shock waves in dilute argon
Phys. Fluids **21**, 066101 (2009); 10.1063/1.3149866

Continuum predictions from molecular dynamics simulations: Shock waves
J. Chem. Phys. **118**, 3161 (2003); 10.1063/1.1537243
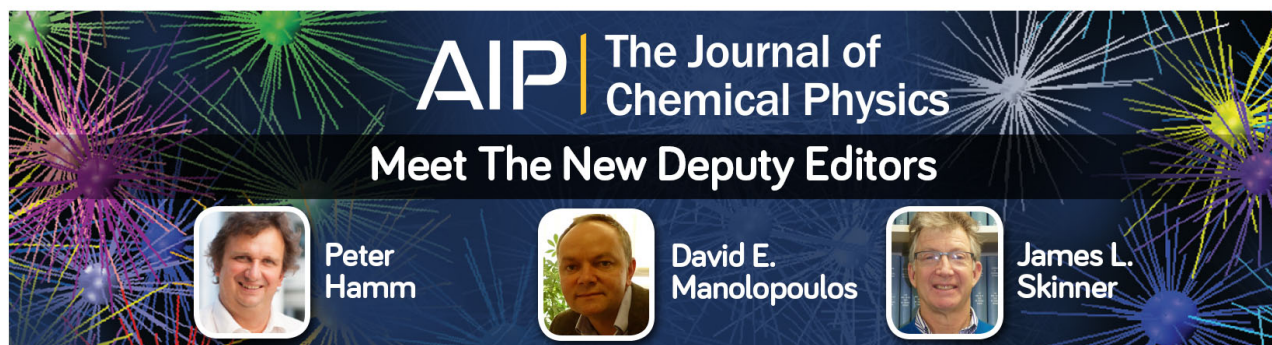
A localized momentum constraint for non-equilibrium molecular dynamics simulations

E. R. Smith, D. M. Heyes, D. Dini,[a)] and T. A. Zaki[b)]
Department of Mechanical Engineering, Imperial College London, Exhibition Road,
South Kensington, London SW7 2AZ, United Kingdom

A method which controls momentum evolution in a sub-region within a molecular dynamics simulation is derived from Gauss's principle of least constraint. The technique for localization is founded on the equations by Irving and Kirkwood [J. Chem. Phys. **18**, 817 (1950)] expressed in a weak form according to the control volume (*CV*) procedure derived by Smith *et al.* [Phys. Rev. E. **85**, 056705 (2012)]. A term for the advection of molecules appears in the derived constraint and is shown to be essential in order to exactly control the time evolution of momentum in the subvolume. The numerical procedure converges the total momentum in the *CV* to the target value to within machine precision in an iterative manner. The localized momentum constraint can prescribe essentially arbitrary flow fields in non-equilibrium molecular dynamics simulations. The methodology also forms a rigorous mathematical framework for introducing coupling constraints at the boundary between continuum and discrete systems. This functionality is demonstrated with a boundary-driven flow test case. © 2015 AIP Publishing LLC. [http://dx.doi.org/10.1063/1.4907880]

I. INTRODUCTION

Since its inception,[1] molecular dynamics (MD) has been applied to a wide range of physical systems and phenomena. A number of technical advances have extended its range of application to different thermodynamic ensembles through the control of the temperature ("thermostat"), pressure ("barostat"), and mass (mass-stat or "pycnostat"). There are a number of thermostats in widespread use including the Andersen,[2] Langevin,[3] Velocity Rescaling,[4] Gaussian,[5] and Nosé-Hoover[6,7] thermostats. There are the Parrinello and Rahman,[8] Butler and Harrowell,[9] and Andersen[2] barostats. For mass control, there are a number of particle insertion techniques such as USHER[10] and FADE[11] as well as mass control by the pycnostat.[12] Control of intermolecular separation is possible using iterative schemes which enforce constraints with algorithms such as SHAKE and its derivatives.[13] Synthetic equations of motion have been proposed to impose flow profiles which act on the entire simulation domain (i.e., the whole periodic cell[8]). These include algorithms such as SLLOD which can enforce a general force distribution and are commonly used to drive planar Couette shear flow.

More recently, MD-Continuum coupling approaches have been developed in which large regions of explicit molecular modelling are replaced by a compatible continuum dynamics (CD) model. While coupling between CD and MD in solids is a mature field,[14,15] coupling for fluid dynamics is still an active area of research. This necessitates a new class of constraints to be applied to a local (Eulerian) region in space rather than the entire molecular domain. A challenging aspect of coupling is devising a technique to guide the molecular region in a manner which matches the continuum evolution at the coupling interface. Since the original work of O'Connell and Thompson,[16] a range of constraint procedures has been developed for this purpose, for example, (a) a force which is derived from a variational principle formulation of mechanics to control state properties (e.g., momentum),[16–18] (b) a numerically favorable control style algorithm,[19] (c) a selectively permeable membrane,[20] (d) a Maxwell-demon type approach,[21] (e) a flux-based (e.g., pressure and advection) constraint constructed from the conservation equations,[22,23] and (f) a constraint derived to minimize entropy by imposing reversible changes through the boundary conditions.[24]

The variety of constraint procedures is a symptom of the underlying challenge: Coupling entails using information from a small set of continuum variables to specify $6N$ molecular degrees of freedom which has a non-unique solution. The choice of coupled variables is also the subject of active research, with schemes grouped into either state coupling (mass, momentum, and energy) or coupling of their fluxes (mass flux, momentum flux, and energy fluxes). Of the many coupling methods, the variational principle approach has a clear physical justification and for this reason is commonly used to derive constraints in the wider MD literature.[5,25,26] The variational principle will therefore form the basis for the constraint derived in this work.

O'Connell and Thompson[16] and Nie *et al.*[18] applied the Principle of Least Action to derive constraint equations. However, examples in the literature demonstrate that the Principle of Least Action, subject to certain constraints, fails to reproduce the Newtonian equations of motion.[27,28] It is therefore not clear that the Principle of Least Action is formally valid for the semi-holonomic constraints of interest here (see Refs. 17, 27, and 29). In contrast, Gauss's principle of least constraint is a true minimum principle, which is applicable to any form

a)Electronic mail: d.dini@imperial.ac.uk
b)Electronic mail: t.zaki@imperial.ac.uk

of constraint.[30] Therefore, Gauss's principle will be applied in this work to confirm the validity of the Principle of Least Action based coupling.

The primary aim of this work is to provide a rigorous technique to localize a constraint to an arbitrary sub-volume embedded within a larger system. In the same way that the definition of pressure in a localized region in an MD simulation is not correctly described by the virial expression (see, for example, Ref. 31), constraints derived without regard to explicit localization can lack formal rigor and lead to spurious property values. The governing equations are differential; in that they equate momentum change over time to fluxes. The introduction of a rigorous localization procedure allows the constrained equations of motion to be applied in the differential form required by the governing equations. It is demonstrated that implementation of constraints in differential form is not possible without explicit localization. Using this procedure, it is shown that the energy added is the same as in the SLLOD equations of motion in the appropriate limit. In addition, the proposed constraint is shown to unify the state and flux literature, by providing a generalized equation which can be reduced to previously proposed state or flux coupling forms. Without simplification, the procedure ensures that both momentum state properties and fluxes are simultaneously enforced. The proposed methodology can be viewed as a framework to develop rigorous localized constraints and would be applicable, for example, to derive localized thermostats.[32]

In the following, Sec. II discusses the continuum control volume (*CV*) equations, the control volume function, and the molecular control volume equations. Section II B presents the derivation of a *CV* localized coupling algorithm using the *CV* function and the principle of least action. In Sec. III, the constrained momentum equations are expressed in discrete form and their convergence properties are evaluated as a function of subdomain size. The constraint is then applied to a boundary-driven flow test case, in Sec. IV, which is also relevant for the study of flow using MD-Continuum coupling. Concluding remarks are provided in Sec. V.

II. THEORY

A localized constraint is sought to guide the evolution of momentum in a region of space embedded within a larger domain. The seminal work by Irving and Kirkwood[33] provides a way of localizing the properties of a discrete molecular system by defining mass, momentum, and energy evolution equations at a point in space (i.e., in the limit of zero volume) using the Dirac delta functional. This is the same limit used for the continuum itself, so the Irving and Kirkwood[33] equations are formally equivalent to the point-wise continuum equations.

The discrete nature of a molecular system hinders direct comparison to the point-wise continuum equations. The difficulty arises because a molecular system is only defined at the locations of molecules.[34] Also, as no molecule is ever exactly located at a given point, the Dirac delta functional used to define continuous properties would always be zero in practice. As a result, the Dirac delta is often replaced by a Gaussian or other smoothed functionals.[35–37] As these functionals have an arbitrary analytic form, the exact equivalence between the

Irving and Kirkwood[33] equations and the continuum equations is lost in this procedure. This loss of equivalence is unimportant when a point in the continuum corresponds to a large finite region in the molecular system. However, for the type of coupled simulation considered in this work, the discrete and continuous systems share the same length and time scales and a smoothed form of the Dirac delta function is not applicable.

To circumvent this problem, the Irving and Kirkwood[33] equations and point-wise continuum equations are both expressed in a mathematically weak form using a control volume. In their weak form, the equations of motion no longer require the point-wise differential equations to hold exactly. For cases where there is the possibility of behavior which violates the continuum assumption, the weakened formulation is arguably the only physically meaningful description.[38,39] Therefore, in this work, all quantities and their time dependence will be expressed in terms of fluxes over the surfaces of a control volume and the temporal changes inside that volume. As a result of using a weakened formulation in both domains, all coupled quantities are well defined, unique and an equivalent form can be obtained in both the discrete and continuum descriptions.

A. Control volume formulation

The control volume formulation is widely used in fluid mechanics because it is exactly conservative. In control volume form, the mass continuity can be expressed as

$$\frac{\partial}{\partial t} \int_V \rho \, dV = -\oint_S \rho \boldsymbol{u} \cdot d\mathbf{S}, \tag{1}$$

where ρ is the mass density, $\boldsymbol{u}$ is the fluid velocity, and $d\mathbf{S} = \mathbf{n} dS$ is the unit normal, $\mathbf{n}$, of the control surface times the area dS. The rate of change of momentum in a *CV* is determined by the advection of momentum and the balance of forces,

$$\frac{\partial}{\partial t} \int_V \rho \boldsymbol{u} \, dV = -\oint_S [\rho \boldsymbol{u}\boldsymbol{u} + \mathbf{\Pi}] \cdot d\mathbf{S} + \mathbf{F}_{\text{body}}, \tag{2}$$

where $\mathbf{\Pi}$ is the pressure tensor on the *CV* surfaces and $\mathbf{F}_{\text{body}}$ accounts for the body forces, such as gravity. The rate of change of energy in the *CV* is the sum of energy advection, $\rho \mathcal{E} \boldsymbol{u}$, pressure heating, $\mathbf{\Pi} \cdot \boldsymbol{u}$, and heat flux, $\boldsymbol{Q}$,

$$\frac{\partial}{\partial t} \int_V \rho \mathcal{E} \, dV = -\oint_S [\rho \mathcal{E} \boldsymbol{u} + \mathbf{\Pi} \cdot \boldsymbol{u} + \boldsymbol{Q}] \cdot d\mathbf{S} + \mathbf{F}_{\text{body}} \cdot \boldsymbol{u}, \tag{3}$$

where $\mathcal{E}$ is the fluid energy. Equations (1)–(3) no longer require the assumption of an infinitesimal volume but express the conservation laws in the form of changes inside a finite volume and the fluxes across its bounding surfaces.

The evolution equations for a molecular system can also be expressed in *CV* form. Only the final form of the Irving and Kirkwood[33] equations in control volume representation is reported here (for a full derivation see Smith *et al.*[40]). Central to obtaining the *CV* form is the three-dimensional integral of the Dirac delta functional,

$$\vartheta_i \equiv \left[H(x^+ - x_i) - H(x^- - x_i) \right]$$
$$\times \left[H(y^+ - y_i) - H(y^- - y_i) \right]$$
$$\times \left[H(z^+ - z_i) - H(z^- - z_i) \right], \tag{4}$$

considered here for a cuboidal subvolume (The choice of integral is arbitrary and other subvolumes can be used, as discussed in Heyes *et al.*[41]). In Eq. (4), x_i is the x coordinate of molecule i, x^+ and x^-, respectively, denote the locations of the top and bottom surfaces of the *CV* in the x direction, and H is the Heaviside functional. Equation (4) selects molecules inside the *CV*, $\vartheta_i = 1$ if molecule i is inside and zero otherwise. The *CV* function, ϑ_i, is a molecular scale equivalent of the continuum control volume and can be used to obtain molecular definitions of continuum style properties. Mass, momentum, and energy are given, respectively, by,

$$N_I \equiv \sum_{i=1}^{N} \vartheta_i; \qquad \int_V \rho \, dV \equiv \sum_{i=1}^{N} m_i \vartheta_i;$$

$$\int_V \rho \boldsymbol{u} \, dV \equiv \sum_{i=1}^{N} m_i \dot{\boldsymbol{r}}_i \vartheta_i; \qquad \int_V \rho \mathcal{E} \, dV \equiv \sum_{i=1}^{N} e_i \vartheta_i, \quad (5)$$

where m_i is the mass, $\dot{\boldsymbol{r}}_i$ is the velocity vector, and $e_i \equiv \frac{p_i^2}{2m_i} + \frac{1}{2}\sum_{j \neq i}^{N} \phi_{ij}$ is the energy of molecule i. Strictly, all definitions should equate the continuum to the ensemble of the MD trajectories, i.e.,

$$\int_V \rho_c \, dV \equiv \sum_{i=1}^{N} \langle m_i \vartheta_i; f \rangle. \quad (6)$$

However, provided that the volume of integration is sufficiently large, the MD-sum provides an accurate representation of the integral of the continuum property over the same volume,

$$\int_V \rho_c \, dV \approx \int_V \rho \, dV = \sum_{i=1}^{N} m_i \vartheta_i. \quad (7)$$

The derivative of the *CV* function with respect to x is

$$dS_{xi} \equiv \frac{\partial \vartheta_i}{\partial x} = \left[\delta(x^+ - x_i) - \delta(x^- - x_i) \right]$$
$$\times \left[H(y^+ - y_i) - H(y^- - y_i) \right]$$
$$\times \left[H(z^+ - z_i) - H(z^- - z_i) \right], \quad (8)$$

which is only non-zero when a molecule i crosses one of the two x surfaces of the *CV*. An analogous *CV* function can be defined by replacing $\boldsymbol{r}_i$ with the line of interaction, $\boldsymbol{r}_i - s\boldsymbol{r}_{ij}$, between two molecules i and j, where $0 < s < 1$. The derivative of this function with respect to x is denoted by $d\mathbf{S}_{ij}$ which selects interactions crossing the x^+ or x^- surfaces of the control volume. Using the *CV* function and its derivative in three dimensions, it is possible to derive discrete analogues of the continuum control volume equations.[40] These include the time evolution of the mass,

$$\frac{d}{dt}\sum_{i=1}^{N} m_i \vartheta_i = -\sum_{i=1}^{N} m_i \dot{\boldsymbol{r}}_i \cdot d\mathbf{S}_i, \quad (9)$$

and the time evolution of momentum (ACCUMULATION), which in the molecular control volume is the sum of surface crossing (ADVECTION) terms and (FORCING) terms consisting of both direct forces from other molecules and external fields $\mathbf{F}_{i_{\text{ext}}}$,

$$\underbrace{\frac{d}{dt}\sum_{i=1}^{N} m_i \dot{\boldsymbol{r}}_i \vartheta_i}_{\text{ACCUMULATION}} = \underbrace{-\sum_{i=1}^{N} m_i \dot{\boldsymbol{r}}_i \dot{\boldsymbol{r}}_i \cdot d\mathbf{S}_i}_{\text{ADVECTION}}$$

$$\underbrace{+ \frac{1}{2}\sum_{i,j}^{N} \boldsymbol{f}_{ij}\vartheta_{ij} + \sum_{i=1}^{N} \mathbf{F}_{i_{\text{ext}}}\vartheta_i}_{\text{FORCING}}. \quad (10)$$

The time evolution of the total energy of the molecules in the control volume is

$$\underbrace{\frac{d}{dt}\sum_{i=1}^{N} e_i \vartheta_i}_{\text{ACCUMULATION}} = \underbrace{-\sum_{i=1}^{N} e_i \dot{\boldsymbol{r}}_i \cdot d\mathbf{S}_i}_{\text{ADVECTION}}$$

$$\underbrace{+ \frac{1}{2}\sum_{i,j}^{N} \dot{\boldsymbol{r}}_i \cdot \boldsymbol{f}_{ij}\vartheta_{ij} + \sum_{i=1}^{N} \dot{\boldsymbol{r}}_i \cdot \mathbf{F}_{i_{\text{ext}}}\vartheta_i}_{\text{FORCING}}. \quad (11)$$

These equations are weak descriptions of the flow in a molecular system, which are formally equivalent to the continuum control volume, given in Eqs. (1)–(3). Just as for their continuum counterparts, these weakened molecular equations give exact conservation in a molecular system with accuracy to machine precision. In Subsection II B, the procedure for controlling the momentum in an arbitrary control volume is described.

B. Localized momentum constraint

In the coupling literature, the original work by O'Connell and Thompson[16] and the subsequent reformulation by Nie *et al.*[18] used the Principle of Least Action. The Principle of Least Action expresses the governing equations in Hamiltonian ($\boldsymbol{q}_i, \boldsymbol{p}_i$) form, where $\boldsymbol{q}_i$ and $\boldsymbol{p}_i$ are the generalized position and momenta three-vectors for molecule i. The equations in Hamiltonian form are useful for determining phase space compressibility and applying linear response theory.[5] However, as the Principle of Least Action is known to give incorrect equations of motions for some constraints,[27] it may not be applicable to obtain a generally valid localized momentum constraint. Gauss's principle of least constraint is used to verify the Principle of Least Action formulation, as in Flannery,[30] because it is applicable to holonomic as well as non-holonomic constraints.[5]

In this section, a method to constrain the momentum in a local region of space, or a control volume, is derived using both the Principle of Least Action and Gauss's principle. The Principle of Least Action gives the equations in Hamiltonian form, and the form obtained from Gauss's principle of least constraint is used to confirm the validity of these equations.[17]

The target of the constraint is to set the difference between the total momentum of a molecular control volume and an equivalent continuum volume to zero, i.e.,

$$\boldsymbol{g}(\boldsymbol{q}, \dot{\boldsymbol{q}}, t) = \sum_{n=1}^{N} m_n \dot{\boldsymbol{q}}_n \vartheta_n - \int_V \rho \boldsymbol{u} \, dV = 0, \quad (12)$$

where $\boldsymbol{q}_n$ is a generalized vector coordinate. Note, the convention used throughout this work is that constrained molecular properties are identified by indices n and m, while i and j are

used for all other molecular indices. Also, the sum of the total momentum in a *CV* is constrained rather than the velocity. The time evolution of momentum is the left hand side of the *CV* momentum balance equation, Eq. (10), and is therefore the natural variable to control. The constraint is applied in the Eulerian reference frame in both MD and continuum regions.

In Secs. II B 1 and II B 2, the constraint of Eq. (12) is applied first using the Principle of Least Action and then Gauss's principle. The two forms are shown to be formally equivalent and the constraint equation is then shown to provide control for all stress and advection terms in the control volume.

1. Principle of least action

The principle of least action states that the motion of a system from time t_1 to t_2 is such that the action $\mathcal{A}$,

$$\mathcal{A} = \int_{t_1}^{t_2} \mathcal{L}_c, \tag{13}$$

is stationary, i.e., $\delta\mathcal{A} = 0$, for the actual path of motion.[17] Here, $\mathcal{L}_c \equiv \mathcal{L} + \boldsymbol{\lambda} \cdot \boldsymbol{g}$ is a Lagrangian with constraint $\boldsymbol{g}$ and $\boldsymbol{\lambda}$ is a Lagrange multiplier to be determined. By minimizing the action, the Euler-Lagrange equation is obtained,[27]

$$\frac{d}{dt} \frac{\partial \mathcal{L}_c}{\partial \dot{\boldsymbol{q}}_i} - \frac{\partial \mathcal{L}_c}{\partial \boldsymbol{q}_i} = 0, \tag{14}$$

which is valid provided the constraint can be shown to be semi-holonomic (see Appendix A and Refs. 27 and 30). The conjugate momentum of molecule i is obtained from the definition

$$\boldsymbol{p}_i \equiv \frac{\partial \mathcal{L}_c}{\partial \dot{\boldsymbol{q}}_i} = m_i \dot{\boldsymbol{q}}_i + m_i \vartheta_i \boldsymbol{\lambda}. \tag{15}$$

The time evolution of the momentum in terms of $\dot{\boldsymbol{p}}_i$ is given by substituting the conjugate momentum, Eq. (15), into the constrained Euler-Lagrange equation, Eq. (14),

$$\dot{\boldsymbol{p}}_i = \frac{\partial \mathcal{L}_c}{\partial \boldsymbol{q}_i} = \boldsymbol{F}_i - \boldsymbol{\lambda} m_i \dot{\boldsymbol{q}}_i \cdot d\mathbf{S}_i. \tag{16}$$

To determine the Lagrange multiplier $\boldsymbol{\lambda}$, $m_i \dot{\boldsymbol{q}}_i$ from Eq. (15) is substituted into the constraint, Eq. (12),

$$\boldsymbol{\lambda} = \frac{1}{\sum_{n=1}^{N} m_n \vartheta_n^2} \left[\sum_{n=1}^{N} \boldsymbol{p}_n \vartheta_n - \int_V \rho \boldsymbol{u} dV \right]. \tag{17}$$

Using the above definition of $\boldsymbol{\lambda}$ in Eqs. (15) and (16) gives the Hamiltonian form of the equations of motion,

$$\dot{\boldsymbol{q}}_i = \frac{\boldsymbol{p}_i}{m_i} - \frac{\vartheta_i}{M_I} \left[\sum_{n=1}^{N} \boldsymbol{p}_n \vartheta_n - \int_V \rho \boldsymbol{u} dV \right], \tag{18a}$$

$$\dot{\boldsymbol{p}}_i = \boldsymbol{F}_i - \frac{m_i \dot{\boldsymbol{q}}_i \cdot d\mathbf{S}_i}{M_I} \left[\sum_{n=1}^{N} \boldsymbol{p}_n \vartheta_n - \int_V \rho \boldsymbol{u} dV \right], \tag{18b}$$

where $M_I \equiv \sum_{n=1}^{N} m_n \vartheta_n$. The key equations for this work, (18a) and (18b), are localized versions of the constraint derived by O'Connell and Thompson,[16] albeit constraining the total momentum instead of velocity. The O'Connell and Thompson[16] constraint is recovered when the *CV* is the entire domain, i.e., $\vartheta_i = 1 \,\forall\, i$ and surface terms, therefore, disappear as $dS_i = 0 \,\forall\, i$. The Hamiltonian form of these Eqs. (18a) and (18b)

can be combined, as shown in Appendix A, to obtain Newton's law including the constraint force explicitly,

$$\ddot{\boldsymbol{q}}_i = \frac{\boldsymbol{F}_i}{m_i} - \frac{\vartheta_i}{M_I}$$
$$\times \left[-\frac{d}{dt} \int_V \rho \boldsymbol{u} dV + \sum_{n=1}^{N} \boldsymbol{F}_n \vartheta_n - \sum_{n=1}^{N} m_n \dot{\boldsymbol{q}}_n \dot{\boldsymbol{q}}_n \cdot d\mathbf{S}_n \right], \tag{19}$$

where the conjugate momentum, $\boldsymbol{p}_i$, has been eliminated from the final expression. In Sec. II B 2, the expression in Eq. (19) is rederived using Gauss's principle.

2. Gauss's principle of least constraint

Assuming a cartesian coordinate system, the generalized coordinates, $\boldsymbol{q}_i$, are replaced by $\boldsymbol{r}_i$. The constraint enforced using Gauss's principle is differential in nature; i.e., it only controls the time change of properties. Therefore, the control volume form of the non-holonomic constraint in Eq. (12) is differentiated with respect to time,

$$\dot{\boldsymbol{g}}(\boldsymbol{r},\dot{\boldsymbol{r}},t) = -\sum_{n=1}^{N} m_n \dot{\boldsymbol{r}}_n \dot{\boldsymbol{r}}_n \cdot d\mathbf{S}_n + \sum_{n=1}^{N} m_n \ddot{\boldsymbol{r}}_n \vartheta_n$$
$$- \frac{d}{dt} \int_V \rho \boldsymbol{u} dV = 0, \tag{20}$$

and introduced into Gauss's principle of least constraint gives

$$\frac{\partial}{\partial \ddot{\boldsymbol{r}}_i} \left[\frac{1}{2} \sum_{n=1}^{N} m_n \left(\ddot{\boldsymbol{r}}_n - \frac{\boldsymbol{F}_n}{m_n} \right)^2 + \boldsymbol{\eta} \cdot \dot{\boldsymbol{g}} \right] = 0, \tag{21}$$

where $\boldsymbol{\eta}$ is a Lagrange multiplier to be determined. Evaluating the derivative in Eq. (21) leads to

$$m_i \ddot{\boldsymbol{r}}_i = \boldsymbol{F}_i - \boldsymbol{\eta} m_i \vartheta_i. \tag{22}$$

Equation (22) is substituted into Eq. (20) to give the following expression for $\boldsymbol{\eta}$:

$$\boldsymbol{\eta} = \frac{1}{M_I} \left[-\frac{d}{dt} \int_V \rho \boldsymbol{u} dV - \sum_{n=1}^{N} m_n \dot{\boldsymbol{r}}_n \dot{\boldsymbol{r}}_n \cdot d\mathbf{S}_n + \sum_{i=1}^{N} \boldsymbol{F}_n \vartheta_i \right]. \tag{23}$$

Substituting $\boldsymbol{\eta}$ into Eq. (22) yields

$$\ddot{\boldsymbol{r}}_i = \frac{\boldsymbol{F}_i}{m_i} - \frac{\vartheta_i}{M_I}$$
$$\times \left[-\frac{d}{dt} \int_V \rho \boldsymbol{u} dV + \sum_{n=1}^{N} \boldsymbol{F}_n \vartheta_n - \sum_{n=1}^{N} m_n \dot{\boldsymbol{r}}_n \dot{\boldsymbol{r}}_n \cdot d\mathbf{S}_n \right], \tag{24}$$

which is identical to Eq. (19). As Gauss's principle is more fundamental,[30] the equivalence of Eqs. (19) and (24) confirms that the application of the Principle of Least Action is physically sound in this case.

This constrained form of Newton's Law, Eq. (24), is a localization of the equations obtained by Nie *et al.*,[18] which have become widely employed in the fluid coupling literature.[42–46] Equation (24) reduces to the Nie *et al.*[18] constraint when the *CV* is the whole domain, $\vartheta_i = 1 \,\forall\, i$, so that the surface flux term vanishes $dS_i = 0 \,\forall\, i$.

The importance of the *CV* localization now becomes evident: without accounting for the advection of every molecule across the control surface, a differential constraint will not be able to prevent a change in momentum within the *CV* (as demonstrated numerically in Sec. III C). Without localization, unchecked molecular advection into and out of the controlled region acts to gradually erode the momentum control applied to the volume. Errors in differential constraints gradually accrue in any numerical implementation. This is a well know problem with Gaussian thermostats and results in temperature drift over time.[5] For the purpose of coupling to a continuum, the drift in momentum quickly renders this method unusable. As a result, a special discretization of the time derivative was applied in the work of Nie *et al.*,[18] which changes the nature of their constraint from purely differential (i.e., controlling only the change of momentum) to a hybrid proportional and differential constraint (i.e., controlling the absolute value of momentum[19]).

The constrained equations of motion, Eqs. (19) and (24), are in differential form when derived from both Gauss's principle of least constraint and the principle of least action. It is therefore the differential form that must be enforced to obtain the correct physical evolution of the system. The inclusion of the momentum flux component in Eq. (24) is key to the success of the localized Gaussian momentum constraint in differential form. That is, only by exactly accounting for all contributions to the momentum within the *CV*, can the differential constraint be successfully applied in a molecular simulation.

3. The constraint equation in terms of fluxes

Constraint equation (24) can be rewritten in the form of Newton's law using an external force, $\boldsymbol{F}_{i_{\text{ext}}}$,

$$m_i \ddot{\boldsymbol{r}}_i = \boldsymbol{F}_i - \boldsymbol{F}_{i_{ext}}, \tag{25}$$

where,

$$\boldsymbol{F}_{i_{ext}} = \frac{m_i \vartheta_i}{M_I} \left[\underbrace{-\frac{d}{dt} \int_V \rho \boldsymbol{u} \, dV}_{\text{CD Accumulation}} + \underbrace{\sum_{n=1}^N \boldsymbol{F}_n \vartheta_n}_{\text{MD Forcing}} \right.$$

$$\left. - \underbrace{\sum_{n=1}^N m_n \dot{\boldsymbol{r}}_n \dot{\boldsymbol{r}}_n \cdot d\boldsymbol{S}_n}_{\text{MD Advection}} \right]. \tag{26}$$

An advantage of this form is that each term has a counterpart in the continuum equations. This provides a starting point for linking the two descriptions. The elements of Eq. (24) can be expressed in terms of a method of planes pressure tensor[47] localized across the *CV* surfaces,[40]

$$\boldsymbol{F}_{i_{ext}} = \frac{m_i \vartheta_i}{M_I} \left[\underbrace{\oint_S \rho \boldsymbol{u}\boldsymbol{u} \cdot d\boldsymbol{S}}_{\text{CD Advection}} + \underbrace{\oint_S \boldsymbol{\Pi} \cdot d\boldsymbol{S}}_{\text{CD Pressure}} \right.$$

$$\left. + \underbrace{\sum_{n,m}^N \boldsymbol{s}_{nm} \cdot d\boldsymbol{S}_{nm}}_{\text{MD Stress}} - \underbrace{\sum_{n=1}^N m_n \dot{\boldsymbol{r}}_n \dot{\boldsymbol{r}}_n \cdot d\boldsymbol{S}_n}_{\text{MD Advection}} \right]. \tag{27}$$

Delgado-Buscalioni and Coveney[48] observed that the flux values at the surface are required to accurately enforce a coupl-

ing scheme. In this context, the constraint expressed in terms of surface fluxes, as in Eq. (27), is the required starting point to derive an accurate flux coupling. Equation (27) can be interpreted as a constraint on all the surface fluxes, and, therefore, the flux coupling methodology of Flekkøy *et al.*[22] is a special case, where computational fluid dynamics (CFD) pressure and advection are applied at the top *CV* surface only and no molecular terms are removed. The localized momentum constraint presented here does not enforce a flux control at each surface separately but only requires that the sum of the flux over all six surfaces of the cubic *CV* be controlled to satisfy Eq. (27). However, if the stress on each surface is individually controlled to the correct value, the total stress from the sum of surfaces will still satisfy Eq. (27).

In this section, Eq. (27) is modified to drive the flux (e.g., stresses) to the required value while ensuring exact control of state (e.g., momentum) properties. The constraint in this form represents a unification of the various coupling schemes defined in the literature and allows coupling of more complex cases which require both state and flux continuities between domains (e.g., two-fluid flow). In deriving a flux control, the pressure in the continuum is split into configurational stress, $\boldsymbol{\sigma}$, and kinetic pressure, $\boldsymbol{\kappa}$, contributions, i.e., $\boldsymbol{\Pi} \equiv \boldsymbol{\kappa} - \boldsymbol{\sigma}$. Only the configurational (stress) components are interpolated, while the kinetic part of the pressure and convection is still treated in a finite volume manner (see, e.g., the discontinuous Galerkin method[49]).

The control of fluxes is achieved by making an appropriate choice of weighting function, which is a standard procedure in the finite element literature.[39] Weighting functions are used to define continuous properties at any point in space by interpolation between nodes (here, the common vertices between *CV*s). In this manner, a continuous stress can be defined at any point in space by interpolating between the known values at the *CV* surfaces in Eq. (27), i.e., for continuum stress,

$$\oint_S \boldsymbol{\sigma}(\boldsymbol{r}) \cdot d\boldsymbol{S} = \oint_S \sum_{a=1}^{\text{nodes}} N_a(\boldsymbol{r}) \tilde{\boldsymbol{\sigma}}_a \cdot d\boldsymbol{S}$$

$$= \int_V \sum_{a=1}^{\text{nodes}} \tilde{\boldsymbol{\sigma}}_a \cdot \boldsymbol{\nabla} N_a(\boldsymbol{r}) dV$$

$$= \sum_{n=1}^N \sum_{a=1}^{\text{nodes}} \tilde{\boldsymbol{\sigma}}_a \cdot \boldsymbol{\nabla} N_a(\boldsymbol{r}_n), \tag{28}$$

where the spatially varying stress, $\boldsymbol{\sigma}$, is replaced by the product of constant nodal stresses and a spatially varying weighting function $\boldsymbol{\sigma}(\boldsymbol{r}) = \sum_a^{\text{nodes}} \tilde{\boldsymbol{\sigma}}_a N_a(\boldsymbol{r})$. In Eq. (28), the choice of weighting function (and how it is applied) is entirely arbitrary provided that the sum of the stresses at the location of the molecules in the *CV* is equal to the sum of the surface stresses on its boundary. As the weighting function must be evaluated at the molecular locations, $\boldsymbol{r}_n$, its form must be carefully selected to ensure this equality (see Appendix B). An example of the simplest choice of weighting functions is provided in Sec. III. The presented framework could also accommodate more complicated functions for N_a, for example, a choice based on the molecular radial distribution function.[50] Having defined a continuously varying stress inside the *CV*, this distributed

stress can be enforced by the constraint, Eq. (27),

$$
\boldsymbol{F}_{i\,\mathrm{ext}} = \frac{m_i \vartheta_i}{M_I} \Bigg[\oint_S \rho \boldsymbol{uu} \cdot d\mathbf{S} + \oint_S \boldsymbol{\kappa} \cdot d\mathbf{S}
$$
$$
- \int_V \sum_{a=1}^{\mathrm{nodes}} [\tilde{\boldsymbol{\sigma}}_a - \tilde{\boldsymbol{\varsigma}}_a] \cdot \boldsymbol{\nabla} N_a dV
$$
$$
- \sum_{n=1}^{N} m_n \dot{\boldsymbol{r}}_n \dot{\boldsymbol{r}}_n \cdot d\mathbf{S}_n \Bigg]. \tag{29}
$$

The distributed force in Eq. (29) is designed to ensure the correct stresses at the *CV* boundary and a linear interpolated value at the location of any molecule *i* between these surfaces. This is achieved by the force which removes the MD stress and applies the desired target continuum stress.

The remainder of this work describes the implementation and application of the constraint force, Eq. (26). In Sec. II C, the momentum is shown to be controlled exactly and the energy properties are discussed.

C. Constraint properties

The constraint force in Eq. (24) is valid for any molecule *i* but is only applied to molecules within the *CV* (i.e., when ϑ_i = 1). The momentum evolution in this *CV* is therefore adjusted to any target value, which can be set from CD or another source. In order to analyze the impact of applying this force to every molecule in a given *CV*, the external force, Eq. (27), is substituted into the momentum equation for the *CV* given by Eq. (10),

$$
\frac{d}{dt} \sum_{i=1}^{N} m_i \dot{\boldsymbol{r}}_i \vartheta_i = - \sum_{i=1}^{N} m_i \dot{\boldsymbol{r}}_i \dot{\boldsymbol{r}}_i \cdot d\mathbf{S}_i + \frac{1}{2} \sum_{i,j}^{N} \boldsymbol{f}_{ij} \vartheta_{ij}
$$
$$
- \sum_{i=1}^{N} \frac{m_i \vartheta_i}{M_I} \Bigg[- \sum_{n=1}^{N} m_n \dot{\boldsymbol{r}}_n \dot{\boldsymbol{r}}_n \cdot d\mathbf{S}_n
$$
$$
+ \frac{1}{2} \sum_{n,m}^{N} \boldsymbol{\varsigma}_{nm} \cdot d\mathbf{S}_{nm}
$$
$$
+ \oint_S \rho \boldsymbol{uu} \cdot d\mathbf{S} + \oint_S \boldsymbol{\Pi} \cdot d\mathbf{S} \Bigg]. \tag{30}
$$

Using the definition of M_I and noting that $\boldsymbol{f}_{nm} \vartheta_{nm} = \boldsymbol{\varsigma}_{nm} \cdot d\mathbf{S}_{nm}$, the molecular *CV* terms cancel and the time evolution of momentum in the constrained *CV* is

$$
\frac{\partial}{\partial t} \sum_{i=1}^{N} m_i \dot{\boldsymbol{r}}_i \vartheta_i = - \oint_S \rho \boldsymbol{uu} \cdot d\mathbf{S} - \oint_S \boldsymbol{\Pi} \cdot d\mathbf{S}. \tag{31}
$$

The constraint applied to a control volume ensures that the molecular momentum evolution is driven by the continuum surface fluxes and forces. From Eq. (2), the right hand side of Eq. (31) is rewritten,

$$
\frac{\partial}{\partial t} \sum_{i=1}^{N} m_i \dot{\boldsymbol{r}}_i \vartheta_i = \frac{\partial}{\partial t} \int_V \rho \boldsymbol{u} dV. \tag{32}
$$

The MD constraint ensures that the temporal evolution of momentum in the MD *CV* is controlled *exactly* to match the target continuum *CV*. As both systems are in *CV* form and the continuum boundary condition is formally equivalent to a constraint, the coupled system can, in principle, be constructed as if the continuum and molecular representations are linked along a common surface.

Having demonstrated that the constraint in Eq. (24) controls the momentum in a *CV* exactly, the resulting energy change in the system is now considered. It is shown that the energy introduced is consistent, in the appropriate limit, with the SLLOD algorithm. The average energy applied to the MD system is obtained by substituting the external force term of Eq. (27) into the energy Eq. (11),

$$
\sum_{i=1}^{N} \dot{\boldsymbol{r}}_i \cdot \boldsymbol{F}_{i\,\mathrm{ext}} \vartheta_i = \frac{1}{M_I} \sum_{i=1}^{N} m_i \vartheta_i \dot{\boldsymbol{r}}_i \cdot \Bigg[\sum_{n,m}^{N} \boldsymbol{\varsigma}_{nm} \cdot d\mathbf{S}_{nm}
$$
$$
- \sum_{n=1}^{N} m_n \dot{\boldsymbol{r}}_n \dot{\boldsymbol{r}}_n \cdot d\mathbf{S}_n
$$
$$
+ \oint_S \rho \boldsymbol{uu} \cdot d\mathbf{S} + \oint_S \boldsymbol{\Pi} \cdot d\mathbf{S} \Bigg]. \tag{33}
$$

Introducing the approximation that the average velocity in a volume is given by the *CV* momenta divided by its mass, Eq. (33) is rewritten as

$$
\sum_{i=1}^{N} \dot{\boldsymbol{r}}_i \cdot \boldsymbol{F}_{i\,\mathrm{ext}} \vartheta_i = -\boldsymbol{\nabla}\boldsymbol{u} : \int_V \Big[(\rho \boldsymbol{uu} + \boldsymbol{\Pi})_{\mathrm{MD}}
$$
$$
- (\rho \boldsymbol{uu} + \boldsymbol{\Pi})_{\mathrm{CD}} \Big] dV + \boldsymbol{u} \cdot \mathbf{F}_{\mathrm{body}}, \tag{34}
$$

where $\boldsymbol{\Pi}_{\mathrm{MD}}$ is the Irving and Kirkwood[33] pressure tensor at a point, which includes the interaction and peculiar momenta components (see Appendix C). The energy added to the system can be compared to the equivalent energy introduced by the SLLOD equations of motion, $\dot{\mathcal{H}}_{\mathrm{SLLOD}} = -\boldsymbol{\nabla}\boldsymbol{u} : \boldsymbol{\Pi}_{\mathrm{MD}}$, which applies homogeneous shear throughout the domain. In this case, the continuum body forces are zero, $\mathbf{F}_{\mathrm{body}} = 0$, and the continuum advection and pressure are constant throughout the domain, $\boldsymbol{u} \cdot \int_V \boldsymbol{\nabla} \cdot (\rho \boldsymbol{uu} + \boldsymbol{\Pi})_{\mathrm{CD}} dV = 0$. Therefore, Eq. (34) reduces to

$$
\sum_{i=1}^{N} \dot{\boldsymbol{r}}_i \cdot \boldsymbol{F}_{i\,\mathrm{ext}} \vartheta_i = -\boldsymbol{\nabla}\boldsymbol{u} : \int_V (\rho \boldsymbol{uu} + \boldsymbol{\Pi})_{\mathrm{MD}} dV. \tag{35}
$$

In the limit that the control volume in Eq. (35) is infinitesimally thin in *y* and of infinite extent in *x* and *z* directions,

$$
\lim_{\Delta x \to \infty} \lim_{\Delta y \to 0} \lim_{\Delta z \to \infty} \boldsymbol{\nabla}\boldsymbol{u} : \int_V (\rho \boldsymbol{uu} + \boldsymbol{\Pi})_{\mathrm{MD}} dV
$$
$$
= \boldsymbol{\nabla}\boldsymbol{u} : \sum_{n,m}^{N} \Big(\boldsymbol{f}_{nm} \boldsymbol{r}_{nm} - m_n \bar{\dot{\boldsymbol{r}}}_n \bar{\dot{\boldsymbol{r}}}_n \Big) \delta(y_n - y). \tag{36}
$$

As SLLOD is applied to the entire domain, it is equivalent to applying a *CV* force on an infinite number of infinitesimally thin control volumes in Eq. (36) throughout the domain. Mathematically, this is the integral of the right hand side of Eq. (36)

performed over the y-axis so

$$-\int_{-\infty}^{\infty} \boldsymbol{\nabla u} : \sum_{n,m}^{N} \left(\boldsymbol{f}_{nm}\boldsymbol{r}_{nm} - m_n \bar{\dot{\boldsymbol{r}}}_n \bar{\dot{\boldsymbol{r}}}_n\right) \delta(y_n - y) dy$$

$$= -\boldsymbol{\nabla u} : \boldsymbol{\Pi}_{\text{MD}} = \dot{\mathcal{H}}_{SLLOD}, \qquad (37)$$

where the advection term, $\rho \boldsymbol{uu}_{\text{MD}}$, cancels between adjacent control volumes. The energy added by the constraint of Eq. (37) is therefore the same as that added by the SLLOD algorithm resulting from the thermodynamic work due to the shear stress.[51] The extra terms in Eq. (33) can, therefore, be interpreted as a generalization of the energy added by the SLLOD algorithm, which includes the advected energy due to constraint localization and energy added for cases where there is a time evolving target velocity. In the coupling literature, there have been attempts to remove the energy added by coupling forces.[24,52,53] However, in a coupled calculation, the energy added to a molecular system should be *exactly* equal to the change of energy in the continuum.

A final consideration is the phase space compressibility,[54,55] which is zero for SLLOD. The expression for the phase space compressibility of Eqs. (18a) and (18b) can be shown to be

$$\Lambda = \frac{(\mathcal{D}-1)}{M_I} \left[\sum_{i=1}^{N} [m_i \vartheta_i - M_I] \boldsymbol{\lambda} \cdot d\mathbf{S}_i - \sum_{i=1}^{N} \boldsymbol{p}_i \vartheta_i \cdot d\mathbf{S}_i\right], \qquad (38)$$

where $\mathcal{D}$ is the dimensionality of the system (see Appendix C). For a control volume equal to the whole volume of the system, $d\mathbf{S}_i = 0$ and consequently $\Lambda = 0$ (i.e., the SLLOD limiting case).

III. IMPLEMENTATION

In this section, practical aspects of the implementation of the local momentum constraint, Eq. (24), are explained and investigated. MD simulations are used to generate molecular trajectories. The total force on the molecule, $\boldsymbol{F}_i = \sum_{i \neq j} \boldsymbol{f}_{ij} = -\sum_{i \neq j} \boldsymbol{\nabla}\Phi_{ij}$ in Eq. (25), is evaluated from the truncated and shifted Lennard-Jones potential (Weeks-Chandler-Andersen, WCA),

$$\Phi(\boldsymbol{r}_{ij}) = \begin{cases} 4\epsilon \left[\left(\dfrac{\ell}{\boldsymbol{r}_{ij}}\right)^{12} - \left(\dfrac{\ell}{\boldsymbol{r}_{ij}}\right)^{6}\right] - 4\epsilon \left[\left(\dfrac{\ell}{\boldsymbol{r}_c}\right)^{12} - \left(\dfrac{\ell}{\boldsymbol{r}_c}\right)^{6}\right], & r_{ij} < r_c \\ 0, & r_{ij} \geq r_c \end{cases}, \qquad (39)$$

where ℓ is the molecular length scale, ϵ is the energy scale, m_i is the mass of molecule i, and $r_{ij} \equiv |\boldsymbol{r}_{ij}|$ where $\boldsymbol{r}_{ij} = \boldsymbol{r}_i - \boldsymbol{r}_j$ is the intermolecular separation. A cutoff length $r_c = 2^{\frac{1}{6}}\ell$ was used beyond which the potential and the applied force are zero. The equations of motion were integrated using the Leapfrog algorithm[56] with a timestep $\Delta t = 0.005$. The software used in these investigations was fully verified and has been used in previous publications.[40,41]

A. Applying the local momentum constraint

The integration of the constrained form of Newton's law, Eq. (25), is performed using Verlet's leapfrog algorithm,[57]

$$\boldsymbol{r}_i(t + \Delta t) = \boldsymbol{r}_i(t) + \Delta t \dot{\boldsymbol{r}}_i(t + \Delta t/2), \qquad (40)$$

$$\dot{\boldsymbol{r}}_i(t + \Delta t/2) = \dot{\boldsymbol{r}}_i(t - \Delta t/2) + \Delta t \boldsymbol{F}_i(\tau)$$

$$-\int_{t-\Delta t/2}^{t+\Delta t/2} \boldsymbol{F}_{i\text{ext}}(\tau) d\tau. \qquad (41)$$

The external force is integrated by identifying the functional dependence of the terms,

$$\boldsymbol{F}_{i\text{ext}} = \frac{m_i \vartheta_i}{M_I} \Bigg[\underbrace{\oint_S [\rho \boldsymbol{uu} + \boldsymbol{\kappa}] \cdot d\mathbf{S}}_{\boldsymbol{F}_{i_{\text{Adv}}}^{\text{CD}}(t)} - \underbrace{\oint_S \boldsymbol{\sigma} \cdot d\mathbf{S} + \sum_{n,m}^{N} \boldsymbol{\varsigma}_{nm} \cdot d\mathbf{S}_{ij}\vartheta_n}_{\boldsymbol{F}_{i_{\text{Stress}}}(\boldsymbol{r}_i, t)}$$

$$-\underbrace{\sum_{n=1}^{N} m_n \dot{\boldsymbol{r}}_n \dot{\boldsymbol{r}}_n \cdot d\mathbf{S}_n}_{\boldsymbol{F}_{i_{\text{Adv}}}^{\text{MD}}(\boldsymbol{r}_i, \dot{\boldsymbol{r}}_i, t)}\Bigg]. \qquad (42)$$

Here, $\boldsymbol{F}_{i_{\text{Adv}}}^{\text{CD}}$ is a force to impose continuum advection, $\boldsymbol{F}_{i_{\text{Stress}}}$ is a force which removes the MD stress and applies the CD stress, while $\boldsymbol{F}_{i_{\text{Adv}}}^{\text{MD}}$ applies the MD advection. The continuum advection terms, $\boldsymbol{F}_{i_{\text{Adv}}}^{\text{CD}}$, depend on time only and can be obtained directly from an external target value (e.g., the continuum) at each time step. Similarly for $\boldsymbol{F}_{i_{\text{Stress}}}$, the continuum component of stress can be obtained from an external source (e.g., the continuum solver). The MD stress component in $\boldsymbol{F}_{i_{\text{Stress}}}$ is dependent on molecular position and can be integrated as

follows:

$$\int\limits_{t-\Delta t/2}^{t+\Delta t/2} \boldsymbol{F}_{i_{\mathrm{Stress}}}[\boldsymbol{r}_i(\tau),\tau]d\tau$$

$$= \int\limits_{t-\Delta t/2}^{t+\Delta t/2} \frac{m_i\vartheta_i[\boldsymbol{r}_i(\tau)]}{M_I[\boldsymbol{r}_i(\tau)]}\left[-\oint_S \boldsymbol{\sigma}\cdot d\mathbf{S}\right.$$

$$\left. + \sum_{n,m}^N \mathbf{S}_{nm}[\boldsymbol{r}_i(\tau)]\cdot d\mathbf{S}_{ij}[\boldsymbol{r}_i(\tau)]\right]d\tau. \quad (43)$$

The integral of the intermolecular forces making up the surface stress term is obtained using the midpoint rule, which has the same order of accuracy as the leapfrog scheme,

$$\int\limits_{t-\Delta t/2}^{t+\Delta t/2} \frac{m_i\vartheta_i[\boldsymbol{r}_i]}{M_I[\boldsymbol{r}_i]}\sum_{n,m}^N \mathbf{S}_{nm}\cdot d\mathbf{S}_{ij}d\tau$$

$$\approx -\Delta t\frac{m_i\vartheta_i[\boldsymbol{r}_i(t)]}{M_I[\boldsymbol{r}_i(t)]}\sum_{n=1}^N \mathbf{S}_{nm}[\boldsymbol{r}_i(t)]\cdot d\mathbf{S}_{ij}[\boldsymbol{r}_i(t)]. \quad (44)$$

The stress force can be applied uniformly to all molecules in the *CV* or in a distributed manner to introduce a flux constraint as discussed in Sec. II B 3. The advection term, $\boldsymbol{F}_{i_{\mathrm{Adv}}}^{\mathrm{MD}}$, is a function of both position and velocity. The integration proceeds by rewriting the Dirac delta function as the sum of its roots and integrating,[58]

$$\int\limits_{t-\Delta t/2}^{t+\Delta t/2} \boldsymbol{F}_{i_{\mathrm{Adv}}}^{\mathrm{MD}}[\boldsymbol{r}_i(\tau),\dot{\boldsymbol{r}}_i(\tau)]d\tau$$

$$= \int\limits_{t-\Delta t/2}^{t+\Delta t/2} \frac{m_i\vartheta_i}{M_I}\sum_{n=1}^N m_n\dot{\boldsymbol{r}}_n(\tau)\dot{\boldsymbol{r}}_n(\tau)\cdot d\mathbf{S}_n(\tau)d\tau$$

$$= \sum_{k=1}^{N_t} \frac{m_i\vartheta_i[\boldsymbol{r}_i(t_k)]}{M_I[\boldsymbol{r}_i(t_k)]}\sum_{n=1}^N \frac{m_n\dot{\boldsymbol{r}}_n(t_k)\dot{\boldsymbol{r}}_n(t_k)}{|\dot{\boldsymbol{r}}_n(t_k)|}\cdot d\mathbf{S}_{n,k}(t_k), \quad (45)$$

where N_t is the number of crossings over the integrated time period and $d\mathbf{S}_{n,k}(t_k)$ is non-zero when molecule n crosses the surface. As with the SHAKE algorithm[13] where positions are iterated until the desired intermolecular bond lengths are

achieved, the velocity dependence of $\boldsymbol{F}_{i_{\mathrm{Adv}}}^{\mathrm{MD}}$ means that the *CV* momentum must be iterated until convergence. The force in Eq. (45) depends on the sum of the momenta of molecules crossing the *CV* surface between $t-\Delta t/2$ and $t+\Delta t$, which moves subject to the constraint. The algorithm is implemented as follows:

```
! Save initial position and velocity of molecules
ri_start = ri; vi_start = vi
! Add integral of intermolecular, CD advective Eq. (43) and stress forces
Eq. (44)
int_F_C = dt*Fi + int_Fi_Adv_CD + int_Fi_Stress
! Iterate until advective force converges for all CV in domain
while (ANY || int_Fi_Adv_MD - int_Fi_Adv_MD_PREV || > ε) do
    int_Fi_Adv_MD = update_MDAdv_force(ri,vi)
    vi = vi_start + int_F_C + int_Fi_Adv_MD
    ri = ri_start + dt*vi
    int_Fi_Adv_MD_PREV = int_Fi_Adv_MD
end while
```

where ϵ is a prescribed tolerance.

The implementation of the momentum constraint algorithm and the rate of convergence are explored next for a range of different sizes of the control volume. Each control volume was constrained to maintain zero change in momentum, so only the MD terms are removed and no continuum terms are added. This test is the simplest possible case as it does not result in a net flow within the molecular domain. The number of iterations necessary to achieve convergence to machine precision was determined for a range of periodic three dimensional MD simulation cells. Five domain sizes were considered, containing 256, 1372, 10 976, 78 732, and 629 856 molecules, respectively. The number of control volumes is kept constant in each simulation, with the MD domain system decomposed into $4\times4\times4$ control volumes in each case. The number of molecules in each *CV*, therefore, increased with the system size (on average, 4, 21, 172, 1136, and 9842 molecules).

The typical convergence times for these five cases are shown in Figure 1(b). The L^2 norm of Eq. (45), the sum of the root mean square change in advection force for every *CV* in the domain, is plotted against the iteration number in Fig. 1(b). The convergence results for a range of iterations are shown (from a simulation of 50 000 iterations). The number of iterations required for convergence is approximately proportional to the surface to volume ratio of the cubic *CV*, since the surface fluxes become relatively less significant as the *CV* size increases. As
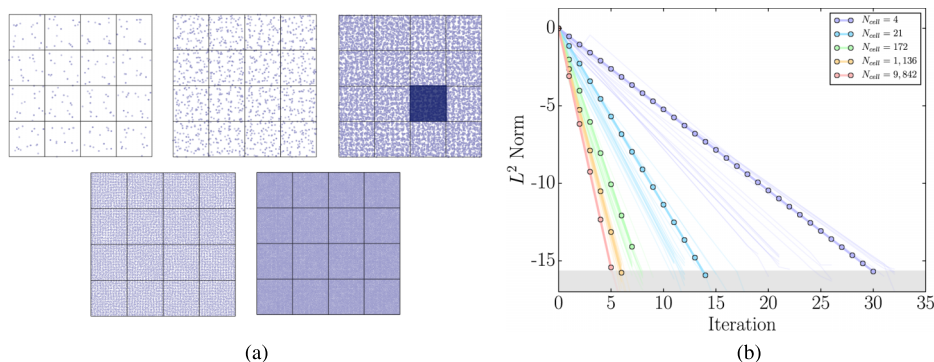
FIG. 1. Example convergence of the *CV* constraint applied to every *CV* in the domain with schematic (left) and results (right). The dark blue square on the schematic indicates the constrained volume used in Sec. III C. The faint lines on the results are convergence at different timesteps and the circles represent a line of best fit to the range of data. Note the lin-log scales. (a) Domain schematic. (b) Convergence.

(a)   (b)

the constraint force is typically applied to a range of contiguous *CV*, the surface flux must be refined by iteration until the constraint force no longer alters the fluxes. Molecules can cross into other *CV* until the flux in each attains the target value within the pre-set tolerance. If a *CV* has no molecules inside it, the momentum is zero by definition. The constraint acts to prevent change in momentum and so will apply a diverging force to prevent the last molecules from leaving. This behavior is entirely consistent with the mathematical formulation of the constraint but can result in numerical instability for small *CV*. Typically, this was found not to be a problem in practice, as in the tests shown in Fig. 1(b) the *CV* with on average 21 molecules and larger is never depleted, even for extreme values of temperature and density.

As the constrained region will typically be a small subset of a larger domain, the fluxes and forces need to be evaluated for only the *M* molecules near any constrained *CV* surface. The *CV* constraint must be applied every timestep, with the total *CV* surface forces calculated from the intermolecular forces and the positions of molecules *i* and *j* using Eq. (44). With a Verlet cell list, this requires a single order *M* calculation of forces per timestep, performed during the main force calculation. The surface momentum fluxes of all *M* molecules must be re-evaluated at each iteration until convergence. The fluxes are obtained from the changes in position of molecule *i* and its velocity using Eq. (45). Surface forces and fluxes are identified in Eqs. (44) and (45) using a combination of Heaviside functionals, which can be implemented in assembly language to improve efficiency.

B. Momentum correction

The applied constraint in Eq. (24) is differential — it only acts on the change of momentum over time. The actual value of the momentum in a *CV* does not need to be specified. As the differential constraint only converges to a given tolerance, ϵ, the absolute value of the momentum will fluctuate about the target value. Provided the tolerance is sufficiently small, these fluctuations are bounded and do not lead to appreciable drift. However, during the simulation, it is sometimes required that the value of the momentum in a *CV* is changed from its current value, $\sum_{i=1}^{N} m_i \dot{r}_i \vartheta_i$, to a perhaps quite different target value, $\int_V (\rho u)_{\text{target}} dV$. A function of time, $f(t)$, can be constructed to implement this change, e.g., a sigmoid-type functional

form,

$$f(t) = \left[\sum_{i=1}^{N} m_i \dot{r}_i(t_1) \vartheta_i(t_1) - \int_V (\rho u)_{\text{target}} dV \right] \tanh\left(\frac{t}{\tau_{\text{correct}}} \right),$$

(46)

where $\tau_{\text{correct}} = t_2 - t_1$ is an arbitrary time period from the start time, t_1, to final time, t_2. The *CV* momentum is the value at time t_1 and the derivative of this expression can then be applied as a force to act on the control volume,

$$F_{\text{prop}} = \frac{m_i \vartheta_i}{M_I} \frac{d}{dt} f(t)$$

$$= \frac{\sum_{i=1}^{N} m_i \dot{r}_i(t_1) \vartheta_i(t_1) - \int_V (\rho u)_{\text{target}} dV}{\tau_{\text{correct}} \cosh^2(t/\tau_{\text{correct}})}.$$

(47)

The effect of this force is to change the total momentum of the *CV* from its value at time, t_1, gradually to the target value. A numerical example of a correction to set the initial momentum of a given *CV* to zero is presented in Sec. III C.

C. Test functions

In this section, the performance of the constraint, Eq. (24), is analyzed for the case when a single *CV* is constrained within a larger periodic domain of WCA molecules. Two types of constraint were applied: the first maintained the CV at zero net momentum and the second applied a sinusoidally varying total momentum. For both constraints, the domain is identical to the middle test case used in Sec. III A, with the constrained *CV* shown by the dark blue square in Fig. 1(a). A total of 10 976 molecules were simulated, and the constrained *CV* containing approximately 172 molecules. The use of a grid of $4 \times 4 \times 4$ control volumes allows the constrained *CV* (number 2,2,2) to be surrounded by a set of adjacent *CV* so that the impact of the periodic boundaries is minimized on all sides.

The first test-case applies a constraint force to prevent the sum of all molecular momenta in a single MD *CV* from varying in time. The momentum correction given in Eq. (47) is used to adjust the initial momentum to a target value of zero over a period of time. The CD Accumulation term is set to zero, i.e., $\frac{d}{dt}\int_V \rho u dV = 0$, and the *CV* momentum in Eq. (30) simplifies to

$$\overbrace{\frac{d}{dt}\sum_{i=1}^{N} m_i \dot{r}_i \vartheta_i}^{\text{ACCUMULATION}} = \overbrace{-\sum_{i=1}^{N} m_i \dot{r}_i \dot{r}_i \cdot d\mathbf{S}_i}^{\text{ADVECTION}} + \overbrace{\frac{1}{2}\sum_{i,j}^{N} f_{ij}\vartheta_{ij}}^{\text{FORCING}} - \underbrace{\sum_{i=1}^{N} \frac{m_i \vartheta_i}{M_I} \left[\underbrace{-\sum_{n=1}^{N} m_n \dot{r}_n \dot{r}_n \cdot d\mathbf{S}_n}_{\text{ADVECTION CONSTRAINT}} + \underbrace{\frac{1}{2}\sum_{n,m}^{N} \boldsymbol{s}_{nm} \cdot d\mathbf{S}_{nm}}_{\text{FORCING CONSTRAINT}} \right]}_{\text{CV CONSTRAINT}}.$$

(48)

The various terms of Eq. (48) are shown for the constrained *CV* in Fig. 2. In order to demonstrate the impact of the constraint, the *CV* Constraint is not applied for the first part of the simu-

lation (before time $t_1 = 0.875$) to allow comparison between constrained and unconstrained evolutions of the system. The Accumulation term can be seen to be equal to the sum of the
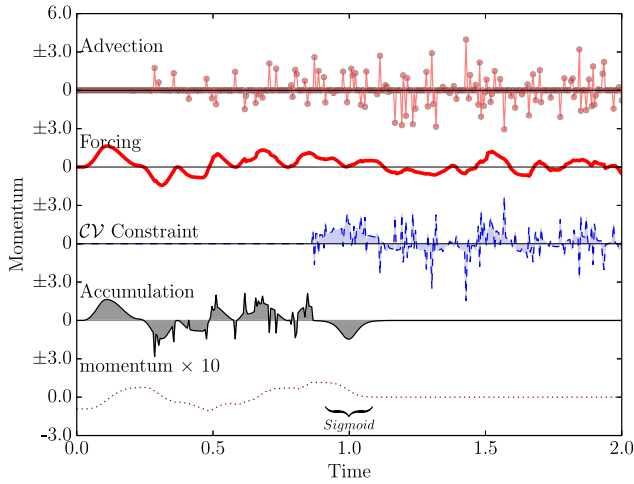
FIG. 2. Summary of the various *CV* components defined in Eq. (48) before and after a constraint is applied. Individual molecular crossings can be seen on the ADVECTION plot, intermolecular forces acting across the *CV* surface on the FORCING plot, and *CV*'s temporal evolution of momentum is shown on the ACCUMULATION plot. The *CV* CONSTRAINT is switched on at $t_1 = 0.875$, applying a sigmoidal function to adjust the *CV* total momentum to zero before acting to exactly cancel the ADVECTION and FORCING terms. As a result, ACCUMULATION is constrained to be zero and momentum no longer changes.

FIG. 3. Summary of the various *CV* components defined in Eq. (49) before and after a sinusoidal constraint is applied. The behavior is as Fig. 2 with the *CV* CONSTRAINT cancelling the *CV*'s natural ADVECTION and FORCING. However, the ACCUMULATION is controlled to evolve cosinusoidally.

ADVECTION and FORCING terms, which is in accordance with Eq. (48) in the absence of the *CV* CONSTRAINT term before t_1 = 0.875. The consequence of a non-zero ACCUMULATION is a freely changing momentum inside the *CV*, shown at 10 times scale on the bottom axis of Fig. 2. The *CV* CONSTRAINT is applied at time $t_1 = 0.875$, so the ADVECTION CONSTRAINT force cancels the ADVECTION term and the FORCING CONSTRAINT term counteracts the FORCING term. This results is the molecular ACCUMULATION being exactly equal to the prescribed evolution of momentum. At first, this ACCUMULATION is changed according to the correction force, Eq. (47), applied over a time period of $\tau_{\text{correct}} = 0.25$. The action of the sigmoid function is to set the momentum to zero in the *CV* between times $t_1 = 0.875$ and $t_2 = 1.125$. After $t_2 = 1.125$, the ACCUMULATION is maintained at zero in the *CV* — in Fig. 2, the *CV* CONSTRAINT can be seen to be equal to the sum of ADVECTION and FORCING in order to enforce this. With the ACCUMULATION kept at zero, the *CV* momentum is maintained at its current value, zero, for the remainder of the simulation. The necessity of the ADVECTION term in the implementation of the control volume constraint, Eq. (48), can be seen from Fig. 2: The applied force must cancel out ADVECTION and FORCING from a *CV* in order for the ACCUMULATION to be zero. Without the ADVECTION term in the *CV* CONSTRAINT, the ACCUMULATION would be equal to ADVECTION and the momentum would not stay at zero. It is for this reason that iteration to obtain the exact ADVECTION CONSTRAINT, outlined in Sec. III A, is essential.

In the next test case, the same *CV* is constrained using a function which enforces a time harmonic evolution of momentum,

$$\frac{d}{dt} \sum_{i=1}^{N} m_i \dot{\boldsymbol{r}}_i \vartheta_i = - \sum_{i=1}^{N} m_i \dot{\boldsymbol{r}}_i \dot{\boldsymbol{r}}_i \cdot d\mathbf{S}_i + \frac{1}{2} \sum_{i,j}^{N} \boldsymbol{f}_{ij} \vartheta_{ij}$$

$$- \sum_{i=1}^{N} \frac{m_i \vartheta_i}{M_I} \left[- \sum_{n=1}^{N} m_n \dot{\boldsymbol{r}}_n \dot{\boldsymbol{r}}_n \cdot d\mathbf{S}_n \right.$$

$$\left. + \frac{1}{2} \sum_{n,m}^{N} \boldsymbol{s}_{nm} \cdot d\mathbf{S}_{nm} + A \cos(2\pi t / \tau_{\text{sin}}) \right], \quad (49)$$

where Eq. (49) is Eq. (48) with the extra term, $\frac{d}{dt} \int_V \rho \boldsymbol{u} dV$ = $A \cos(2\pi t / \tau_{\text{sin}})$, added to enforce an oscillatory ACCUMULATION to the *CV*. The amplitude of the oscillation is set to $A = 2.0$ and the time constant to $\tau_{\text{sin}} = 0.5$. As in the previous example, the *CV* constraint is zero for the first part of the simulation. The constraint is again applied at time $t_1 = 0.875$, with the same sigmoid function as given in Eq. (47) with $\tau_{\text{correct}} = 0.25$, used to set the initial momentum to zero. In Fig. 3, the *CV* constraint can be seen to apply both ADVECTION constraint and FORCING constraint terms as before, with an extra cosine based driving term. The applied constraint results in a sinusoidal evolution of momentum in the *CV* which exactly matches the expected momentum evolution obtained from the integral of the driving term in Eq. (49), namely, $\int [\frac{d}{dt} \int_V \rho \boldsymbol{u} dV] dt = \frac{A\tau}{2\pi} \sin(2\pi t / \tau)$.

D. Stress constraint

This section demonstrates the use of a distributed force to apply the varying continuum stress introduced in Sec. II B 3. An example of the implementation of the distributed force of Eq. (27) is shown in Fig. 4. The direction of the applied stress on the boundaries of the *CV* is indicated by the set of blue arrows in Fig. 4. The applied force is then distributed by an appropriate choice of interpolating weight function, N_a, for node a to enforce this stress at each of the surfaces. The simplest value for $\boldsymbol{\nabla} N_a$ in Eq. (28) which can implement this stress on six surfaces of the *CV* is the product of three one-dimensional linear shape functions. Here, $\boldsymbol{\nabla} N_a$ = $\prod_{\beta=x,y,z} (1 - \omega_{a\beta} \omega_\beta)$ with $\omega_\beta = (r_\beta - r_\beta^-)/\Delta r_\beta$ and $\omega_{a\beta}$ is the value at node a. The stress at the eight nodes of the cubic control volume is obtained from the three intersecting surfaces
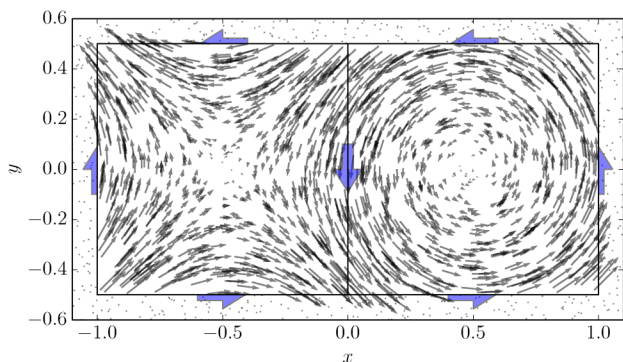
FIG. 4. Two dimensional linear force distribution applied by specified *CV* surface stresses. The stresses on the left cell enforce shear and the stresses on the right rotation. The forces on molecules outside the *CV* are zero.

taking only the internal values to the current *CV*, for example, $\tilde{\sigma}_{x1} = \sigma_{xy}^- + \sigma_{xx}^- + \sigma_{xz}^-$ and $\nabla N_1 = (1 - \omega_x)(1 - \omega_y)(1 - \omega_z)$. The resulting force is displayed using vectors at molecular locations, whose size is proportional to the respective force magnitudes. The left hand *CV* is subjected to two dimensional shear stretching while the right *CV* surface stresses apply a rotational flow. For this demonstration, the applied force is the same on the shared surface between the two *CV*s.

The arbitrary nature of the weighting functions implies that the sum of the forces on all molecules in the *CV* will only approximate the left hand side of Eq. (28). However, in order to maintain exact momentum control which is required for state coupling, this sum of forces on all *CV* molecules must equal the sum of the *CV* surface stresses exactly (as demonstrated by Fig. 2). This can be thought of as a further boundary condition. To satisfy this condition, the order of the weighting function ∇N_a must be increased from linear to quadratic. Appendix B explains a general method to design a shape function which ensures the correct sum inside the *CV* and the correct stress at the *CV* boundaries. A constraint in this form thereby simultaneously implements both state and flux based coupling.

Figure 4 only shows the effect of enforcing simple two dimensional stress profiles. However, it is possible to specify the eighteen surface stress components to match complicated three dimensional stress distributions imposed from the external boundaries (e.g., continuum fields). Each of the three stress components on the six surfaces of the cubic control volume can be specified, allowing the constraint to define combinations of rotations, shearing, elongation, and compression. This could be particularly useful for embedded coupling schemes,[59,60] which aim to track a deforming periodic (Lagrangian) domain driven by boundary shear.[61] Applying a shear with sliding or deforming boundaries often becomes insurmountably complex in three dimensions.[60] The key strength of the treatment presented here stems from the use of the fixed (Eulerian) framework where molecules are free to enter and leave as a result of the applied stress.

IV. RESULTS

In Sec. III, the coupled constraint of Eq. (25) was applied to several simple flow fields. In this section, the constraint

method is applied to control the molecular system as part of a coupled simulation. The application of direct coupling using a continuum solver demonstrates all aspects of the constraint methodology together, including application of a sigmoid function, stress control and enforcing the complex momentum evolution of the molecules in multiple *CV*. The target stresses and momenta are supplied by a simple two-dimensional finite volume solver which simulates evolving Couette flow. The methodology presented could be used with any finite volume code, such as $\mathcal{T}rans\mathcal{F}low$.[62–65]

In the case of coupling, the molecular and continuum regions should act as a single contiguous domain. Therefore, the constraint applied at the top boundary of the molecular region should drive the flow as if it was directly joined to the continuum domain. The process of coupling introduces a number of extra sources of complexity, including an open boundary on the MD domain and the potential insertion of molecules. Only one-way coupling is presented, as the performance of the constraint force on the *CV* is the focus of this work. The CFD solver implements the momentum balance of Eq. (2) with the total pressure tensor split into kinetic and stress components $\mathbf{\Pi} = \boldsymbol{\kappa} - \boldsymbol{\sigma}$ such that

$$\frac{\partial}{\partial t} \int_V \rho \boldsymbol{u} \, dV = -\oint_S [\rho \boldsymbol{uu} + \boldsymbol{\kappa} - \boldsymbol{\sigma}] \cdot d\mathbf{S}. \qquad (50)$$

For the case of Couette flow, it is assumed that there is negligible net convective flux, $\oint_S \rho \boldsymbol{uu} \cdot d\mathbf{S} \approx 0$, and no kinetic contribution (i.e., $\boldsymbol{\kappa} = 0$). Discretizing Eq. (50) using the finite volume[66] methodology gives

$$\rho \Delta V \frac{\boldsymbol{u}(t + \Delta t) - \boldsymbol{u}(t)}{\Delta t} = + \sum_{f=1}^{6} \boldsymbol{\sigma}_f \cdot \boldsymbol{n}_f \Delta S_f, \qquad (51)$$

where the summation in f is over the six cubic finite volume surfaces with area ΔS_f. The density, $\rho = 0.8$, is assumed to be constant and the integrated velocity in a volume on the left hand side is discretized using a simple forward Euler approximation. The stress on each surface is obtained by assuming that the fluid is Newtonian, so that $\boldsymbol{\sigma} = \mu d\boldsymbol{u}/d\boldsymbol{r}$ where $\mu = 1.6$ is the viscosity.[67] The finite volume methodology is conservative in the same manner as the *CV* constraint derived in this work. As a result, the sum of the surface stresses on the right hand side of Eq. (51) determines the time evolution of the left hand side exactly. By simply applying these stresses to the MD system, the time evolution of the momentum should exactly match the CFD time evolution with no further correction required. In addition, the stresses are applied in a distributed manner using the method described in Sec. III D. The timestep, Δt = 0.005, and system sizes, $\Delta x = 11.91, \Delta y = 5.87$, in MD units are chosen to match the MD solver. The CFD has four cells in the *x* (streamwise) direction with periodic boundaries enforced by halo cells.[66] There are ten cells in the *y* (wall-normal) direction, two of which are halo cells to set the boundary conditions. These halo cells are used to match the molecular wall with $u = 0$ at the bottom and $u = 1$ at the top. As the code is two dimensional, the *z* (spanwise) direction essentially acts as a single cell with periodic images either side.

The CFD and the MD parts of the procedure are solved on separate processors with data exchange implemented using the open source `CPL_library`.[68] Three components of velocity

and the eighteen stresses on each volume are sent from the CFD solver at each timestep. As the CFD is only two dimensional, the undefined third-dimensional surfaces are set to zero and therefore do not contribute to the constraint.

The MD domain is matched in size to the continuum solver with the y (wall-normal) direction bounded by tethered walls. The MD domain is split into 10 CV, to match the 10 cells in the CFD. The y (wall-normal) direction has four coupled CV as shown by the red molecules on Fig. 5(a). This extends by four CV in the x and z ($\Delta x = 11.91, \Delta z = 11.91$) directions with periodic boundary condition applied. The x CVs are shown at half their actual size on Fig. 5(a).

The top and bottom volumes correspond to the CFD halos and contain the wall of tethered atoms. These walls have a density of $\rho_w = 1.0$ and are slightly smaller than the CV, with a height of 4 reduced units, which accounts for the stick-slip behaviour at the wall in the MD, a phenomenon not accounted for in the CFD treatment. The top wall is given a constant sliding velocity of $U_w = 1.0$ and the bottom wall does not translate. The molecular system is initialized with a temperature of unity, $T_0 = 1.0$, and both walls are controlled to this temperature by a Nosé-Hoover (NH) thermostat, which is only applied to the wall atoms.[26,32] The complete set of equations of motion implemented in the MD system is

$$\dot{\boldsymbol{r}}_i = \frac{\bar{\boldsymbol{p}}_i}{m_i} + U_w \mathbf{n}_x, \tag{52a}$$

$$\dot{\bar{\boldsymbol{p}}}_i = \boldsymbol{F}_i + \boldsymbol{F}_{i_{\text{teth}}} - \xi \bar{\boldsymbol{p}}_i + \sum_{C=1}^{N_C} \boldsymbol{F}_{i_{\text{ext}}}^C, \tag{52b}$$

$$\boldsymbol{F}_{i_{\text{ext}}}^C = \frac{m_i \vartheta_i^C}{M_I^C} \left[\frac{d}{dt} \int_{V^C} \rho \boldsymbol{u} dV^C - \sum_{n=1}^N \left(\boldsymbol{F}_n \vartheta_n^C \right. \right.$$
$$\left. \left. - m_n \dot{\boldsymbol{r}}_n \dot{\boldsymbol{r}}_n \cdot d\mathbf{S}_n^C \right) \right], \tag{52c}$$

$$\boldsymbol{F}_{i_{\text{teth}}} = \boldsymbol{r}_{i_0} \left(4k_4 r_{i_0}^2 + 6k_6 r_{i_0}^4 \right), \tag{52d}$$

$$\dot{\boldsymbol{r}}_{i_0} = U_w \mathbf{n}_x, \tag{52e}$$

$$\dot{\xi} = \frac{1}{Q_\xi} \left[\sum_{n=1}^N \frac{\bar{\boldsymbol{p}}_n \cdot \bar{\boldsymbol{p}}_n}{m_n} - 3T_0 \right], \tag{52f}$$

where the constraint force is applied over all constrained cells N_C. Here, $\mathbf{n}_x$ is the unit vector in the x direction and $\boldsymbol{F}_{i_{\text{teth}}}$ is the tethered atom force, obtained using the coefficients of Petravic and Harrowell[69] (with coefficients $k_4 = 5 \times 10^3$ and $k_6 = 5 \times 10^6$). All masses are assumed equal, $m_i \equiv m$ for convenience. The thermostat damping coefficient was set to $Q_\xi = N\Delta t$ so it applies a thermostat which is proportional to the number of molecules, N, in the system. The vector, $\boldsymbol{r}_{i_0} = \boldsymbol{r}_i - \boldsymbol{r}_0$, is the displacement of the tethered atom, i, from its lattice site coordinate, $\boldsymbol{r}_0$. The atom's current position, $\boldsymbol{r}_i$, and that of its tethered site, $\boldsymbol{r}_{i_0}$, slide with the same velocity.

The sigmoid style correction force in Eq. (47) is applied initially to remove the molecular noise and corrects the CV to the CFD starting values. After this, the time evolution in the CV is ensured by applying the CFD surface stresses only.

The surface stresses in the finite-volume continuum solver determine the time evolution of the CFD momentum at the next timestep exactly (Eq. (51)). As a result, the total momentum in each constrained CV of Fig. 5 (red) evolves identically to the corresponding continuum CV. There are no fluctuations in the mean momentum of the constrained region and it will match the continuum analytical solution to the same accuracy as the CFD algorithm. The uncontrolled CVs in the bottom half of the domain (blue) are driven indirectly by interaction with molecules in the constrained region at the top. As a result, momentum measured in the unconstrained region will evolve as in a boundary-driven molecular simulation. Mean quantities show good agreement with the continuum analytical solution but molecular fluctuations are observed.

A common criticism of Gaussian style constraints is that they are too aggressive, destroying the natural hydrodynamic fluctuation present in a molecular simulation.[26] To ensure this is not the case, the probability density functions for the x-velocity in a constrained (red, top fluid cell with mean velocity approximately one) and unconstrained (blue, bottom fluid cell with mean velocity approximately zero) CVs are compared in Fig. 5(b). Good agreement is observed relative to the expected analytical form of the distribution, with indistinguishable impact on the distributions in both the constrained and unconstrained regions. Therefore, the use of a Gaussian constraint is seen to preserve the natural fluctuations in the molecular system while providing exact control of momentum evolution.

(a)   (b)
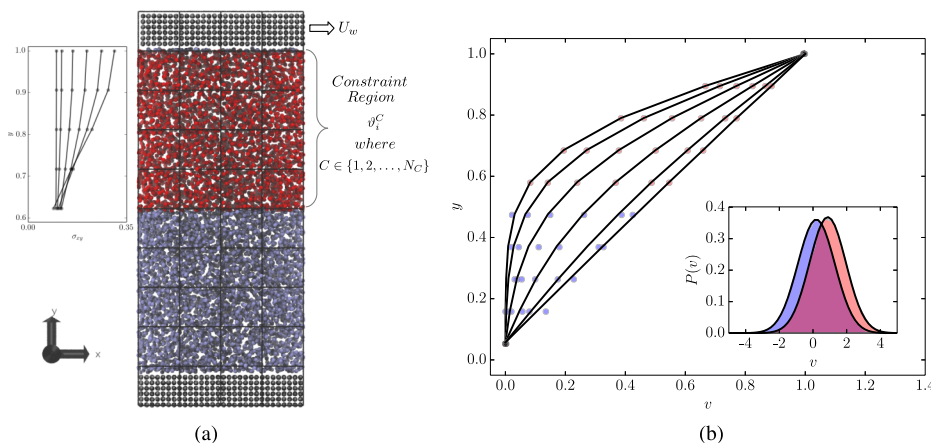
FIG. 5. The geometrical setup and results from the Couette flow case. In all figures, red denotes constrained and blue unconstrained. The black lines are analytical solutions, for Couette flow[40] and Gaussian solution at the same temperature and velocity for the probability density functions (PDF). (a) Couette schematic with example CV shown and applied stress profile from CFD, applied as forces to the MD. (b) The velocity evolution of Couette flow in the MD system compared to the analytical solution at successive times. The x-velocity PDF for constrained (top fluid CV, red) and unconstrained (bottom fluid CV, blue) domain CVs are in the inset.

V. CONCLUSIONS

A method is presented to control momentum in any localized region of a molecular simulation. Localization is achieved using an integrated Dirac delta function, a technique motivated by the *CV* formulation widely used in continuum mechanics. Minimization principles are employed to guarantee the constrained equations of motion are physically meaningful. The resulting equations are proved to exactly control the time evolution of momentum. Furthermore, the energy added by the constraint is shown to be consistent with the SLLOD algorithm. These schemes are preferred to Nosé Hoover style constraints, in some cases, as they allow the **exact** matching of the system's evolution required for coupled continuum-molecular models, non-canonical ensembles and rapidly varying non-equilibrium molecular dynamics simulations.

It is demonstrated that the formal localization process is essential to ensure exact mathematical control of momentum. The exact control is enforced in finite precision numerics by iteration to machine precision. As the momentum constraint is enforced using the sum of the molecular fluxes on a *CV*, it is shown that stresses can also be prescribed by controlling individual *CV* surfaces. The resulting manipulation of the state of stress in the system provides simultaneous state (momentum) and flux (stress) controls. This unifies a number of schemes in the continuum-molecular coupling literature.

Using the localized constraint, the control of momentum and stress is applied to a range of simple test cases. These tests demonstrate each of the features of the constraint, including control of momentum to machine precision, exact manipulation of time evolution of momentum, and application of arbitrary stress profiles. Finally, direct coupling to a continuum solver is demonstrated, bringing all the features of the constraint together to enforce exact evolution in line with the continuum solution of time evolving Couette flow.

ACKNOWLEDGMENTS

APPENDIX A: REFORMULATING HAMILTONIAN EQUATIONS IN TERMS OF NEWTON'S LAW

In this appendix, the details of combining Hamiltonian Eqs. (18a) and (18b), to obtain a form of Newton's law, Eq. (19), are provided. Differentiating Eq. (18a) and substituting the resulting expression in Eq. (18b) yield

$$\ddot{\boldsymbol{q}}_i = \frac{\boldsymbol{F}_i}{m_i} - \dot{\boldsymbol{\lambda}}\vartheta_i, \tag{A1}$$

where the definition of $\boldsymbol{\lambda}$ comes from Eq. (17). The time derivative of the *CV* function $d\vartheta_i/dt = -\dot{\boldsymbol{q}}_i \cdot d\mathbf{S}_i$ cancels with the surface flux in Eq. (18b) (a consequence of the constraint satisfying the semi-holonomic condition[27]). The time derivative of $\boldsymbol{\lambda}$ is

$$\dot{\boldsymbol{\lambda}} = \frac{1}{M_I} \left[\underbrace{\frac{d}{dt} \sum_{n=1}^{N} \boldsymbol{p}_n \vartheta_n - \frac{d}{dt} \int_V \rho \boldsymbol{u} dV}_{\mathcal{A}} \right.$$

$$\left. + \frac{\boldsymbol{\lambda}}{M_I} \sum_{n=1}^{N} m_n \dot{\boldsymbol{q}}_n \cdot d\mathbf{S}_n \right]. \tag{A2}$$

The $\mathcal{A}$ term can be re-written using Eqs. (18a) and (18b) as

$$\mathcal{A} = \frac{d}{dt} \sum_{n=1}^{N} \boldsymbol{p}_n \vartheta_n = \sum_{n=1}^{N} \left[\dot{\boldsymbol{p}}_n \vartheta_n - \boldsymbol{p}_n \dot{\boldsymbol{q}}_n \cdot d\mathbf{S}_n \right]$$

$$= \sum_{n=1}^{N} \left[\boldsymbol{F}_n \vartheta_n - m_n \dot{\boldsymbol{q}}_n \dot{\boldsymbol{q}}_n \cdot d\mathbf{S}_n \right]$$

$$- \boldsymbol{\lambda} \sum_{n=1}^{N} \left[m_n \vartheta_n \dot{\boldsymbol{q}}_n \cdot d\mathbf{S}_n \right.$$

$$\left. + m_n \vartheta_n \dot{\boldsymbol{q}}_n \cdot d\mathbf{S}_n \right],$$

so that the time evolution of the Lagrange multiplier becomes

$$\dot{\boldsymbol{\lambda}} = \frac{1}{M_I} \left[\sum_{n=1}^{N} \boldsymbol{F}_n \vartheta_n - \sum_{n=1}^{N} m_n \dot{\boldsymbol{q}}_n \dot{\boldsymbol{q}}_n \cdot d\mathbf{S}_n - \frac{d}{dt} \int_V \rho \boldsymbol{u} dV \right]$$

$$+ \frac{\boldsymbol{\lambda}}{M_I} \left[\sum_{n=1}^{N} m_n \dot{\boldsymbol{q}}_n \cdot d\mathbf{S}_n - 2 \sum_{n=1}^{N} m_n \vartheta_n \dot{\boldsymbol{q}}_n \cdot d\mathbf{S}_n \right]. \tag{A3}$$

Using $\vartheta_n d\mathbf{S}_n = 1/2 d\mathbf{S}_n$, the second term on the right hand side of Eq. (A3) is zero and inserting the remaining terms into the equation of motion, of Eq. (A1), gives

$$\ddot{\boldsymbol{q}}_i = \frac{\boldsymbol{F}_i}{m_i} - \frac{\vartheta_i}{M_I} \left[\sum_{n=1}^{N} \boldsymbol{F}_n \vartheta_n - \sum_{n=1}^{N} m_n \dot{\boldsymbol{q}}_n \dot{\boldsymbol{q}}_n \cdot d\mathbf{S}_n \right.$$

$$\left. - \frac{d}{dt} \int_V \rho \boldsymbol{u} dV \right], \tag{A4}$$

which is Eq. (19) in the main text.

APPENDIX B: DERIVATION OF A NON-LINEAR WEIGHTING FUNCTION

In this appendix, a general method for deriving three-dimensional weighting functions is presented to enforce both state and flux couplings, as discussed in Sec. III D. The objective is to design a function which has the correct values at the surfaces while maintaining an exact sum for an arbitrary selection of molecules. For a function of the form

$$f(x) = ax^2 + bx + c, \tag{B1}$$

we seek the coefficients a, b, and c which enforce the boundary conditions

$$f(x = 0) = b_{BC} \rightarrow c = b_{BC},$$

$$f(x = 1) = t_{BC} \rightarrow a + b + c = t_{BC},$$

$$\sum_{n=1}^{N} f(x_n) = s_{BC} \rightarrow a \sum_{n=1}^{N} x_n^2 + b \sum_{n=1}^{N} x_n + Nc = s_{BC}.$$

This can be solved exactly to yield,

$$a = \frac{s_{BC} - Nc - [t_{BC} - b_{BC}] \sum x_n}{\sum (x_n^2 - x_n)}$$

$$b = -\frac{s_{BC} - Nc - [t_{BC} - b_{BC}] \sum x_n^2}{\sum (x_n^2 - x_n)}. \tag{B2}$$

In practice, the weighting functions employed by finite element methods are three-dimensional, derived from the product of three one-dimensional functions. However, the third boundary condition on $\sum_{n=1}^{N} f(x_n)$ cannot be applied in the same manner in two or more dimensions, since the coordinates are no longer independent, i.e.,

$$\sum_{n=1}^{N} f(x_n) f(y_n) = s_{BC} \rightarrow \left[a_x \sum_{n=1}^{N} x_n^2 + b_x \sum_{n=1}^{N} x_n + Nc_x \right]$$

$$\times \left[a_y \sum_{n=1}^{N} y_n^2 + b_y \sum_{n=1}^{N} y_n + Nc_y \right] = s_{BC}.$$

For two or more dimensions, a different approach is required, starting with a linear function defined as

$$h(x) = bx + c,$$

which must satisfy the top and bottom boundary conditions,

$$h(x = 0) = b_{BC} \rightarrow c = b_{BC},$$
$$h(x = 1) = t_{BC} \rightarrow b = t_{BC} - b_{BC}.$$

Next, a second-order function is added which is zero at both boundaries, e.g.,

$$g(x) = \left(x - \frac{1}{2}\right)^2 - \frac{1}{4} = x^2 - x, \tag{B3}$$

with a coefficient a tuned to ensure that the boundary condition is satisfied,

$$\sum_{n=1}^{N} [ag(x_n) + h(x_n)] = a \sum_{i=1}^{N} [x_n^2 - x_n] + [t_{BC} - b_{BC}]$$

$$\times \sum_{i=1}^{N} x_n + Nb_{BC} = s_{BC}. \tag{B4}$$

The value for a can be solved,

$$a = \frac{s_{BC} - Nb_{BC} - [t_{BC} - b_{BC}] \sum x_n}{\sum (x_n^2 - x_n)}, \tag{B5}$$

which is equivalent to the direct solution of Eq. (B2) in the one-dimensional case. However, the advantage of this procedure is clear in three dimensions. In each dimension, an independent linear shape function, h, can be defined with coefficients satisfying the respective boundary conditions. The three-dimensional weighting function is the product of three one-dimensional functions, $h(x)h(y)h(z)$. The sum boundary condition,

$$\sum_{n=1}^{N} h(x_n) h(y_n) h(z_n) = s_{BC} + E_{lin}, \tag{B6}$$

can be enforced by defining, E_{lin}, an error term to be eliminated. A second-order term can then be added with coefficient tuned to

remove the error, E_{lin}, and ensure the sum boundary condition,

$$a \sum_{i=1}^{N} [x_n^2 - x_n] [y_n^2 - y_n] [z_n^2 - z_n] = E_{lin}. \tag{B7}$$

This process can be used for *any* shape function employed to distribute stresses at discrete location, by adding a function of higher order to force the sum to be correct.

APPENDIX C: ENERGY EQUATION AND PHASE SPACE COMPRESSIBILITY

In this section, the energy added by the constraint is derived, along with the phase space compressibility. Starting from the energy added by the external constraint, Eq. (33), the terms can be manipulated as follows. Using the constraint, Eq. (12), the sum of molecular momenta can be re-written in terms of the continuum *CV* counterparts. The average velocity components in a volume are then approximately the continuum *CV* momenta divided by the mass of that volume,

$$\frac{1}{M_I} \int_V \rho \boldsymbol{u} \, dV \approx \boldsymbol{u}. \tag{C1}$$

The molecular pressure tensor and advection can be expressed as

$$\sum_{n=1}^{N} (\boldsymbol{F}_n \vartheta_n - m_n \dot{\boldsymbol{r}}_n \dot{\boldsymbol{r}}_n \cdot d\mathbf{S}_n)$$

$$= -\oint_S \rho \boldsymbol{uu} \cdot d\mathbf{S} - \sum_{n=1}^{N} m_n \bar{\dot{\boldsymbol{r}}}_n \bar{\dot{\boldsymbol{r}}}_n \cdot d\mathbf{S}_n + \sum_{n,m}^{N} \boldsymbol{\varsigma}_{nm} \cdot d\mathbf{S}_{nm}$$

$$\equiv \oint_S (\rho \boldsymbol{uu} + \boldsymbol{\Pi})_{MD} \cdot d\mathbf{S} = \int_V \boldsymbol{\nabla} \cdot (\rho \boldsymbol{uu} + \boldsymbol{\Pi})_{MD} dV, \tag{C2}$$

while the continuum time evolutions from Eq. (2) are

$$\frac{d}{dt} \int_V \rho \boldsymbol{u} \, dV = -\oint_S (\rho \boldsymbol{uu} + \boldsymbol{\Pi})_{CD} \cdot d\mathbf{S} + \mathbf{F}_{body}$$

$$= -\int_V \boldsymbol{\nabla} \cdot (\rho \boldsymbol{uu} + \boldsymbol{\Pi})_{CD} + \mathbf{F}_{body}. \tag{C3}$$

Therefore, Eq. (33) becomes

$$\sum_{i=1}^{N} \dot{\boldsymbol{r}}_i \cdot \boldsymbol{F}_{i_{ext}} \vartheta_i = -\boldsymbol{u} \cdot \int_V \boldsymbol{\nabla} \cdot \left[(\rho \boldsymbol{uu} + \boldsymbol{\Pi})_{MD} \right.$$

$$\left. - (\rho \boldsymbol{uu} + \boldsymbol{\Pi})_{CD} \right] dV + \boldsymbol{u} \cdot \mathbf{F}_{body}. \tag{C4}$$

Using the fundamental theorem of the calculus to move the divergence outside the integral, this is equivalent to

$$\sum_{i=1}^{N} \dot{\boldsymbol{r}}_i \cdot \boldsymbol{F}_{i_{ext}} \vartheta_i = -\boldsymbol{\nabla} \boldsymbol{u} : \int_V \left[(\rho \boldsymbol{uu} + \boldsymbol{\Pi})_{MD} \right.$$

$$\left. - (\rho \boldsymbol{uu} + \boldsymbol{\Pi})_{CD} \right] dV + \boldsymbol{u} \cdot \mathbf{F}_{body}, \tag{C5}$$

by rearranging the dot product. Note that the energy added by the CD advection and pressure is only non-zero when these terms vary throughout the domain, i.e., $\boldsymbol{u} \cdot \int_V \boldsymbol{\nabla} \cdot (\rho \boldsymbol{uu} + \boldsymbol{\Pi})_{CFD} dV \neq 0$.

The phase space compressibility, Λ, is obtained as follows. The Hamiltonian form of the equations of motion Eqs. (18a)

and (18b) can be rewritten using the definition of $\boldsymbol{\lambda}$ from Eq. (17),

$$\dot{\boldsymbol{p}}_i = \boldsymbol{F}_i - [\boldsymbol{p}_i - m_i \vartheta_i \boldsymbol{\lambda}] \, \boldsymbol{\lambda} \cdot d\mathbf{S}_i$$

$$= \boldsymbol{F}_i - \boldsymbol{p}_i \boldsymbol{\lambda} \cdot d\mathbf{S}_i + \frac{1}{2} m_i \boldsymbol{\lambda}\boldsymbol{\lambda} \cdot d\mathbf{S}_i, \qquad (C6)$$

where $\vartheta_i d\mathbf{S}_i = 1/2 d\mathbf{S}_i$ has been applied. Phase space compressibility is defined as

$$\Lambda = \sum_{i=1}^{N} \left[\frac{\partial}{\partial \boldsymbol{p}_i} \cdot \dot{\boldsymbol{p}}_i + \frac{\partial}{\partial \boldsymbol{r}_i} \cdot \dot{\boldsymbol{r}}_i \right], \qquad (C7)$$

which requires the derivative of $\boldsymbol{\lambda}$, with respect to momentum and positions. First, the derivative with respect to momentum is evaluated,

$$\frac{\partial}{\partial \boldsymbol{p}_i} \cdot \boldsymbol{\lambda} = \frac{1}{M_I} \sum_{n=1}^{N} \vartheta_n \frac{\partial}{\partial \boldsymbol{p}_i} \cdot \boldsymbol{p}_n = \frac{\mathcal{D}\vartheta_i}{M_I}, \qquad (C8)$$

where $\mathcal{D}$ is the dimensionality of the space (here $\mathcal{D} = 3$). Next, the derivative of $\boldsymbol{\lambda}$ with respect to position is obtained,

$$\frac{\partial}{\partial \boldsymbol{r}_i} \cdot \boldsymbol{\lambda} = \frac{\partial M_I^{-1}}{\partial \boldsymbol{r}_i} \cdot \left[\sum_{n=1}^{N} \boldsymbol{p}_n \vartheta_n - \int_V \rho \boldsymbol{u} \, dV \right]$$

$$+ \frac{1}{M_I} \frac{\partial}{\partial \boldsymbol{r}_i} \cdot \left[\sum_{n=1}^{N} \boldsymbol{p}_n \vartheta_n - \int_V \rho \boldsymbol{u} \, dV \right], \qquad (C9)$$

where the derivative of M_I^{-1}, using $\vartheta_i d\mathbf{S}_i = 1/2 d\mathbf{S}_i$, is

$$\frac{\partial M_I^{-1}}{\partial \boldsymbol{r}_i} = -M_I^{-2} \frac{\partial}{\partial \boldsymbol{r}_i} \sum_{n=1}^{N} m_n \vartheta_n^2 = \frac{m_i d\mathbf{S}_i}{M_I^2} \qquad (C10)$$

and Eq. (C9) becomes

$$\frac{\partial}{\partial \boldsymbol{r}_i} \cdot \boldsymbol{\lambda} = \frac{1}{M_I} [m_i \boldsymbol{\lambda} - \boldsymbol{p}_i] \cdot d\mathbf{S}_i. \qquad (C11)$$

Substituting Eqs. (C8) and (C11) into Eq. (C7), the phase space compressibility is, therefore,

$$\Lambda = \sum_{i=1}^{N} \left[\frac{\partial}{\partial \boldsymbol{p}_i} \cdot \left(\boldsymbol{F}_i - [\boldsymbol{p}_i - m_i \vartheta_i \boldsymbol{\lambda}] \, \boldsymbol{\lambda} \cdot d\mathbf{S}_i \right) \right.$$

$$\left. + \frac{\partial}{\partial \boldsymbol{r}_i} \cdot \left(\frac{\boldsymbol{p}_i}{m_i} - \vartheta_i \boldsymbol{\lambda} \right) \right]$$

$$= \sum_{i=1}^{N} \Big[-\underbrace{\frac{\partial}{\partial \boldsymbol{p}_i} \cdot (\boldsymbol{p}_i \boldsymbol{\lambda} \cdot d\mathbf{S}_i)}_{\mathcal{A}_i} + \underbrace{\frac{1}{2} \frac{\partial}{\partial \boldsymbol{p}_i} \cdot (m_i \boldsymbol{\lambda}\boldsymbol{\lambda} \cdot d\mathbf{S}_i)}_{\mathcal{B}_i}$$

$$- \underbrace{\frac{\partial}{\partial \boldsymbol{r}_i} \cdot (\vartheta_i \boldsymbol{\lambda})}_{C_i} \Big]. \qquad (C12)$$

Some further manipulation is required to simplify Eq. (C12). Working term by term, $\mathcal{A}_i$ can be expanded using Eq. (C8),

$$\mathcal{A}_i = \frac{\partial}{\partial \boldsymbol{p}_i} \cdot (\boldsymbol{p}_i \boldsymbol{\lambda} \cdot d\mathbf{S}_i) = \left[\boldsymbol{\lambda} \frac{\partial}{\partial \boldsymbol{p}_i} \cdot \boldsymbol{p}_i + \boldsymbol{p}_i \frac{\partial}{\partial \boldsymbol{p}_i} \cdot \boldsymbol{\lambda} \right] \cdot d\mathbf{S}_i$$

$$= \mathcal{D} \left[\boldsymbol{\lambda} + \frac{\boldsymbol{p}_i \vartheta}{M_I} \right] \cdot d\mathbf{S}_i. \qquad (C13)$$

The $\mathcal{B}_i$ term can be re-expressed using Eq. (C8),

$$\mathcal{B}_i = \frac{1}{2} \frac{\partial}{\partial \boldsymbol{p}_i} \cdot (m_i \boldsymbol{\lambda}\boldsymbol{\lambda} \cdot d\mathbf{S}_i) = m_i \boldsymbol{\lambda} \cdot d\mathbf{S}_i \frac{\partial}{\partial \boldsymbol{p}_i} \cdot \boldsymbol{\lambda}$$

$$= \frac{\mathcal{D} m_i \vartheta_i \boldsymbol{\lambda} \cdot d\mathbf{S}_i}{M_I}. \qquad (C14)$$

Finally, employing Eq. (C11) to re-write C_i,

$$C_i = \frac{\partial}{\partial \boldsymbol{r}_i} \cdot (\vartheta_i \boldsymbol{\lambda}) = -\boldsymbol{\lambda} \cdot d\mathbf{S}_i + \vartheta_i \frac{\partial}{\partial \boldsymbol{r}_i} \cdot \boldsymbol{\lambda}$$

$$= \frac{\vartheta [m_i \boldsymbol{\lambda} - \boldsymbol{p}_i] \cdot d\mathbf{S}_i}{M_I} - \boldsymbol{\lambda} \cdot d\mathbf{S}_i. \qquad (C15)$$

Substituting the expressions for $\mathcal{A}_i$, $\mathcal{B}_i$, and C_i into Eq. (C12),

$$\Lambda = \sum_{i=1}^{N} \left(-\mathcal{D} \left[\boldsymbol{\lambda} + \frac{\boldsymbol{p}_i \vartheta_i}{M_I} \right] \cdot d\mathbf{S}_i + \frac{\mathcal{D} m_i \vartheta_i \boldsymbol{\lambda} \cdot d\mathbf{S}_i}{M_I} \right.$$

$$\left. - \vartheta_i \frac{[m_i \boldsymbol{\lambda} - \boldsymbol{p}_i] \cdot d\mathbf{S}_i}{M_I} + \boldsymbol{\lambda} \cdot d\mathbf{S}_i \right) \qquad (C16)$$

and rearranging yields the phase space compressibility, Λ,

$$\Lambda = \frac{(\mathcal{D} - 1)}{M_I} \sum_{i=1}^{N} (m_i \boldsymbol{\lambda} \vartheta_i - \boldsymbol{p}_i \vartheta_i - M_I \boldsymbol{\lambda}) \cdot d\mathbf{S}_i. \qquad (C17)$$

[1] B. J. Alder and T. E. Wainwright, "Phase transition for a hard sphere system," J. Chem. Phys. **27**, 1208 (1957).
[2] H. C. Andersen, "Molecular dynamics simulations at constant pressure and/or temperature," J. Chem. Phys. **72**, 2384 (1980).
[3] M. P. Allen and D. J. Tildesley, *Computer Simulation of Liquids*, 1st ed. (Clarendon Press, Oxford, 1987).
[4] S. I. Sandler and L. V. Woodcock, "Historical observations on laws of thermodynamics," J. Chem. Eng. Data **55**(10), 4485 (2010).
[5] D. J. Evans and G. P. Morriss, *Statistical Mechanics of Non-Equilibrium Liquids*, 2nd ed. (Australian National University Press, Canberra, 2007).
[6] S. Nosé, "A molecular dynamics method for simulations in the canonical ensemble," Mol. Phys. **52**(2), 255 (1984).
[7] W. G. Hoover, "Canonical dynamics: Equilibrium phase-space distributions," Phys. Rev. A **31**, 1695 (1985).
[8] M. Parrinello and A. Rahman, "Crystal structure and pair potentials: A molecular-dynamics study," Phys. Rev. Lett. **45**, 1196 (1980).
[9] S. Butler and P. Harrowell, "Simulation of the coexistence of a shearing liquid and a strained crystal," J. Chem. Phys. **118**(9), 4115 (2003).
[10] R. Delgado-Buscalioni and P. V. Coveney, "Usher: An algorithm for particle insertion in dense fluids," J. Chem. Phys. **119**, 978 (2003).
[11] M. K. Borg, D. A. Lockerby, and J. M. Reese, "The fade mass-stat: A technique for inserting or deleting particles in molecular dynamics simulations," J. Chem. Phys. **140**(7), 074110 (2014).
[12] B. A. Dalton, P. J. Daivis, J. S. Hansen, and B. D. Todd, "Effects of nanoscale density inhomogeneities on shearing fluids," Phys. Rev. E **88**, 052143 (2013).
[13] J. P. Ryckaert and A. Bellemans, "Molecular dynamics of liquid n-butane near its boiling point," Chem. Phys. Lett. **30**(1), 123 (1975).
[14] W. A. Curtin and R. E. Miller, "Atomistic/continuum coupling in computational material science," Modell. Simul. Mater. Sci. Eng. **11**, 33 (2003).
[15] D. Davydov, J.-P. Pelteret, and P. Steinmann, "Comparison of several staggered atomistic-to-continuum concurrent coupling strategies," Comput. Methods Appl. Mech. Eng. **277**, 33 (2014).
[16] S. T. O'Connell and P. A. Thompson, "Molecular dynamics-continuum hybrid computations: A tool for studying complex fluid flow," Phys. Rev. E **52**, R5792 (1995).
[17] H. Goldstein, C. Poole, and J. Safko, *Classical Mechanics*, 3rd ed. (Addison Wesley, Boston, 2002).
[18] X. B. Nie, S. Y. Chen, W. N. E, and M. O. Robbins, "A continuum and molecular dynamics hybrid method for micro- and nano-fluid flow," J. Fluid Mech. **500**, 55 (2004).
[19] M. K. Borg, G. B. Macpherson, and J. M. Reese, "Controllers for imposing continuum-to-molecular boundary conditions in arbitrary fluid flow geometries," Mol. Simul. **36**, 745 (2010).

20J. Li, D. Liao, and S. Yip, "Coupling continuum to molecular-dynamics simulation: Reflecting particle method and the field estimator," Phys. Rev. E **57**, 7259 (1997).

21N. G. Hadjiconstantinou, "Hybrid atomistic continuum formulations and the moving contact-line problem," Ph.D. thesis (MIT, US, 1998).

22E. G. Flekkøy, G. Wagner, and J. Feder, "Hybrid model for combined particle and continuum dynamics," Europhys. Lett. **52**, 271 (2000).

23R. Delgado-Buscalioni and P. V. Coveney, "Continuum-particle hybrid coupling for mass, momentum, and energy transfers in unsteady fluid flow," Phys. Rev. E **67**, 046704 (2003).

24E. G. Flekkøy, R. Delgado-Buscalioni, and P. V. Coveney, "Flux boundary conditions in particle simulations," Phys. Rev. E **72**, 026703 (2005).

25M. E. Tuckerman, *Statistical Mechanics: Theory and Molecular Simulation*, 1st ed. (Oxford University Press, 2010).

26W. G. Hoover, *Computational Statistical Mechanics*, 1st ed. (Elsevier Science, Oxford, 1991).

27M. R. Flannery, "The enigma of nonholonomic constraints," Am. J. Phys. **73**(3), 265 (2005).

28I. R. Gatland, "Nonholonomic constraints: A test case," Am. J. Phys. **72**(7), 941 (2004).

29H. Goldstein, C. Poole, and J. Safko, *Errata, Corrections and Comments on Classical Mechanics*, 3rd ed. (Addison Wesley, Boston, 2010), URL: http://astro.physics.sc.edu/Goldstein/.

30M. R. Flannery, "D'alembert–Lagrange analytical dynamics for nonholonomic systems," J. Math. Phys. **52**(3), 032705 (2011).

31D. M. Heyes, E. R. Smith, D. Dini, H. A. Spikes, and T. A. Zaki, "Pressure dependence of confined liquid behavior subjected to boundary-driven shear," J. Chem. Phys. **136**, 134705 (2012).

32S. Bernardi, B. D. Todd, and D. J. Searles, "Thermostating highly confined fluids," J. Chem. Phys. **132**(24), 244706 (2010).

33J. H. Irving and J. G. Kirkwood, "The statistical mechanics theory of transport processes. IV. The equations of hydrodynamics," J. Chem. Phys. **18**, 817 (1950).

34M. Zhou, "A new look at the atomic level virial stress: On continuum-molecular system equivalence," Proc. R. Soc. London **459**, 2347 (2003).

35L. B. Lucy, "A numerical approach to the testing of the fission hypothesis," Astron. J. **82**(12), 1013 (1977).

36Wm. G. Hoover and C. G. Hoover, "Tensor temperature and shock-wave stability in a strong two-dimensional shock wave," Phys. Rev. E **80**(1), 011128 (2009).

37R. M. Puscasu, B. D. Todd, P. J. Daivis, and J. S. Hansen, "An extended analysis of the viscosity kernel for monatomic and diatomic fluids," J. Phys.: Condens. Matter 195105 (2010).

38O. Kolditz, *Computational Methods in Environmental Fluid Mechanics*, 1st ed. (Springer-Verlag, Berlin, 2002).

39O. C. Zienkiewicz, *The Finite Element Method: Its Basis and Fundamentals*, 6th ed. (Elsevier, Butterworth-Heinemann, Oxford, 2005).

40E. R. Smith, D. M. Heyes, D. Dini, and T. A. Zaki, "Control-volume representation of molecular dynamics," Phys. Rev. E. **85**, 056705 (2012).

41D. M. Heyes, E. R. Smith, D. Dini, and T. A. Zaki, "The method of planes pressure tensor for a spherical subvolume," J. Chem. Phys. **140**(5), 054506 (2014).

42X. B. Nie, S. Y. Chen, and M. O. Robbins, "Hybrid continuumatomistic simulation of singular corner flow," Phys. Fluids **16**, 3579 (2004).

43T. H. Yen, C. Y. Soong, and P. Y. Tzeng, "Hybrid molecular dynamics-continuum simulation for nano/mesoscale channel flows," Microfluid. Nanofluid. **3**, 665 (2007).

44J. Sun, Y. He, and W. Tao, "Scale effect on flow and thermal boundaries in micro-/nano-channel flow using molecular dynamicscontinuum hybrid simulation method," Int. J. Numer. Methods Eng. **81**, 207 (2010).

45J. Sun, Y. He, W. Tao, X. Yin, and H. Wang, "Roughness effect on flow and thermal boundaries in microchannel/nanochannel flow using molecular dynamics-continuum hybrid simulation," Int. J. Numer. Methods Eng. **89**, 2 (2012).

46Y. C. Wang and G. W. He, "A dynamic coupling model for hybrid atomistic-continuum computations," Chem. Eng. Sci. **62**, 3574 (2007).

47B. D. Todd, D. J. Evans, and P. J. Daivis, "Pressure tensor for inhomogeneous fluids," Phys. Rev. E **52**, 1627 (1995).

48R. Delgado-Buscalioni and P. V. Coveney, "Hybrid molecular-continuum fluid dynamics," Philos. Trans. R. Soc. London **362**, 1639 (2004).

49F. Bassi and S. Rebay, "High-order accurate discontinuous finite element solution of the 2d Euler equations," J. Comput. Phys. **138**(2), 251–285 (1997).

50T. Werder, J. H. Walther, and P. Koumoutsakos, "Hybrid atomistic continuum method for the simulation of dense fluid flows," J. Comput. Phys. **205**, 373 (2005).

51Wm. G. Hoover, C. G. Hoover, and J. Petravic, "Simulation of two- and three-dimensional dense-fluid shear flows via nonequilibrium molecular dynamics: Comparison of time-and-space-averaged stresses from homogeneous Doll's and Sllod shear algorithms with those from boundary-driven shear," Phys. Rev. E **78**, 046701 (2008).

52J. Liu, S. Chen, X. Nie, and M. O. Robbins, "A continuumatomistic simulation of heat transfer in micro- and nano-flows," J. Comput. Phys. **227**(1), 279 (2007).

53G. Wagner, E. Flekky, J. Feder, and T. Jossang, "Coupling molecular dynamics and continuum dynamics," Comput. Phys. Commun. **147**, 670 (2002).

54F. Frascoli, D. J. Searles, and B. D. Todd, "Chaotic properties of planar elongational flow and planar shear flow: Lyapunov exponents, conjugate-pairing rule, and phase space contraction," Phys. Rev. E **73**, 046206 (2006).

55E. G. D. Cohen, "Transport coefficients and Lyapunov exponents," Physica A **213**(3), 293–314 (1995).

56D. C. Rapaport, *The Art of Molecular Dynamics Simulation*, 2nd ed. (Cambridge University Press, Cambridge, 2004).

57L. Verlet, "Computer "experiments" on classical fluids. I. Thermodynamical properties of Lennard-Jones molecules," Phys. Rev. **159**, 98 (1967).

58P. J. Daivis, K. P. Travis, and B. D. Todd, "A technique for the calculation of mass, energy and momentum densities at planes in molecular dynamics simulations," J. Chem. Phys. **104**, 9651 (1996).

59W. Ren and W. E, "Heterogeneous multiscale method for the modeling of complex fluids and micro fluidics," J. Comput. Phys. **204**, 1 (2005).

60S. Yasuda and R. Yamamoto, "A model for hybrid simulations of molecular dynamics and computational fluid dynamics," Phys. Fluids **20**(11), 113101 (2008).

61A. W. Lees and S. F. Edwards, "The computer study of transport processes under extreme conditions," J. Phys. C: Solid State Phys. **5**, 1921 (1972).

62T. A. Zaki, J. G. Wissink, W. Rodi, and P. A. Durbin, "Direct numerical simulations of transition in a compressor cascade: The influence of free-stream turbulence," J. Fluid Mech. **665**, 57 (2010).

63K. P. Nolan and T. A. Zaki, "Conditional sampling of transitional boundary layers in pressure gradients," J. Fluid Mech. **728**, 306–339 (2013).

64T. A. Zaki, "From streaks to spots and on to turbulence: Exploring the dynamics of boundary layer transition," Flow, Turbul. Combust. **91**, 451 (2013).

65T. O. Jelly, S. Y. Jung, and T. A. Zaki, "Turbulence and skin friction modification in channel flow with streamwise-aligned superhydrophobic surface texture," Phys. Fluids **26**(9), 095102 (2014).

66C. Hirsch, *Numerical Computation of Internal and External Flows*, 2nd ed. (Elsevier, Oxford, 2007).

67M. C. Potter and D. C. Wiggert, *Mechanics of Fluids*, 3rd ed. (Brooks/Cole, California, 2002).

68E. R. Smith and D. Trevelyan, Cpl-library, May 2013, URL: http://code.google.com/p/cpl-library/.

69J. Petravic and P. Harrowell, "The boundary fluctuation theory of transport coefficients in the linear-response limit," J. Chem. Phys. **124**, 014103 (2006).